NOAA TECHNICAL MEMORANDUM NWS CR-94

THE REMOVAL OF STAGNANT WINTER AIR MASSES FROM WYOMING'S WIND RIVER BASIN

Gary L. Cox
National Weather Service Forecast Office
Cheyenne, Wyoming

Jeffrey M. Graham
National Weather Service Office
Lander, Wyoming

November 1988

UNITED STATES DEPARTMENT OF COMMERCE
C. William Verity, Jr.
Secretary

National Oceanic and Atmospheric Administration
William E. Evans
Under Secretary

National Weather Service
Elbert W. Friday, Jr.
Assistant Administrator

TABLE OF CONTENTS

	Page No.
Abstract	1
1. Introduction	1
2. Formation of Inversions	3
3. Theoretical Background	4
A. Destabilization	4
B. Dynamic Instability	5
4. Case Studies	6
A. November 15, 1986--Inversion Break	6
B. December 30, 1986--Inversion Break	17
C. December 27, 1986--Inversion Failed to Break	25
5. Discussion	31
A. Moist Richardson Number	31
B. Influence of Gravity Waves	36
6. Summary	41
7. Acknowledgements	42
8. References	42

THE REMOVAL OF STAGNANT WINTER AIR MASSES FROM WYOMING'S WIND RIVER BASIN

Gary L. Cox
National Weather Service Forecast Office
Cheyenne, Wyoming

Jeffrey M. Graham[1]
National Weather Service Office
Lander, Wyoming

Abstract. A common forecast problem during late fall through early spring in Wyoming is the scouring of a shallow dome of cold air from the Wind River Basin. If there is sufficient snow cover to serve as a radiative sink, cold air filtering into the Basin following the passage of a cold front will become trapped and stagnant. These air masses are characterized by a very steep, surface-based radiation inversion 300 to 500 feet deep, capped by a much deeper subsidence inversion. They are removed only by the passage of another cold front of sufficient strength to increase the vertical wind shear and decrease the static stability so that dynamic instability occurs. Observational evidence is presented that suggests a gradient Richardson number of about 0.7 can is needed to produce this dynamic instability.

1. Introduction

One of the recurring forecast problems during late fall through early spring in Wyoming is the scouring of a shallow dome of cold air from the Wind River Basin. The Wind River Basin is located in the west-central part of the state (Fig. 1). The cold air, typically only a few hundred feet deep during the afternoons, keeps the high temperatures at Lander (LND) and Riverton (RIW) only in the single digits or teens, while at higher level locations in the Wind River Range maximum temperatures are in the 20's, 30's and even lower 40's.

An even more serious concern than the discomfort and cost of the persistent cold is the trapping and accumulation of atmospheric pollutants in the shallow dome of air. In especially long episodes, like during the severe winter of 1983-1984, Fremont County authorities have had to ban the burning of wood in heating stoves.

Another problem associated with the inversions, most commonly in the Riverton area near the confluence of a couple of rivers, is very dense, persistent fog which poses a threat to travelers. Road conditions are also slow to improve because of the cold.

---

[1] Current affiliation is National Weather Service Forecast Office, Great Falls, Montana.

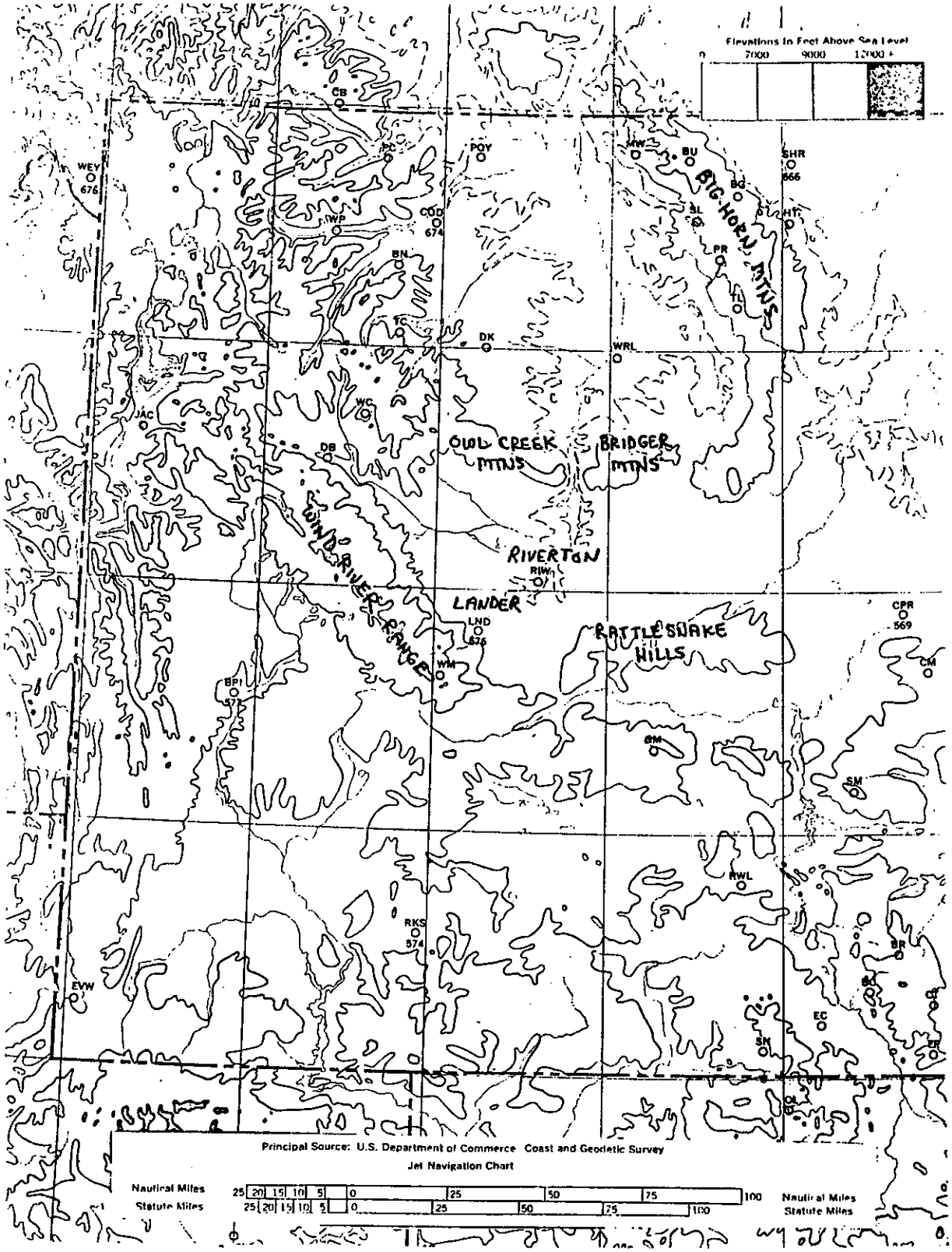

Fig. 1. Topographical features of central and western Wyoming. Horizontal distance scale at base of map and elevation scale at upper right.

By "scouring of the cold air," the authors mean enough of a decrease in the static stability of the stagnant cold air mass for it to be replaced by a newer Pacific or Canadian air mass. When this occurs, the steep surface (or near surface) inverted temperature stratum is mixed out. Rules of thumb for forecasting the scouring of the cold air range from guessing at the potential strength of an approaching weather system to waiting until the Lander temperature starts warming at a rate of 10 to 20°F per hour and then updating the forecast. This paper presents an attempt to quantify approaching disturbances, specifically cold fronts, in terms of characteristics such as vertical wind shear and gradient Richardson Number in hopes that this will provide a reliable indication whether the approaching cold air mass will replace the stagnant one in the Wind River Basin. While it is a curious meteorological situation, we are concerned with determining whether a passing cold front is strong enough to warm the Basin up.

2. Formation of Inversions

Typically, a subsidence inversion is present after a cold air mass moves into the Wind River Basin from the north or east under the anticyclonic portion of an upper tropospheric storm system. Following the clearing of skies and drying of the air behind the storm, a surface-based radiative inversion develops due to night-time cooling. The strength, depth, and persistence of this inversion is partially dependent on the depth of snow cover. This is due to the strong reflection of solar energy (high albedo) and strong radiation of terrestrial energy (high emissivity) (Munn, 1966). Depending on water content, as little as 2 percent of the incident radiation will penetrate a depth of 10 cm (four inches) into the snow (Sellers, 1965). In all the cases used for this study, the snow cover was more than three inches.

The topography of the Basin facilitates the pooling of the cold air. Along the Popo Agie (pronounced PO-PO-SHA') River, flowing northeastward from Lander to Riverton, the elevations are about 5,500 feet MSL (Fig. 1). Between Lander and Riverton the Popo Agie merges with the Wind and Little Wind rivers, which approach from the west. The resultant Wind River then flows north through the Wind River Canyon. The terrain rises steadily in all directions from the rivers.

A large gap between the Big Horn Mountains northeast of Riverton and the Rattlesnake Hills to the east-southeast allows cold air masses to back into the Basin. Also, smaller gaps in the Owl Creek Mountains to the north-northwest of Riverton and the Bridger Mountains to the north-northeast allow cold air masses to funnel in. Figure 1 shows how strongly the elevations rise north, west and south of the Basin.

The surface-based inversions deepen and become shallower with the diurnal cycle. On 12 UTC soundings, the top of the radiation inversion is frequently from 800 to 780 mb (a height of 1,000 to 1,500 feet AGL). During the day the top of the radiation inversion lowers to within 300 to 500 feet of the surface, or to a pressure of 810 to 820 mb.

As one would expect, the greatest increase in temperature off the surface is noted on the 12 UTC soundings. When the inversions are at their most persistent, inversion rates of 45°C km^{-1} are common, especially just before inversion break. Rates as high as 95°C km^{-1} were found in this study. These extreme surface-based values were noted after warming above the boundary layer had occurred in association with an air mass moving in from the Pacific Northwest.

After cold air has settled into the Wind River Basin, the normal configuration of the Lander sounding is a radiational inversion up to around 800 mb, topped by another weaker inversion or isothermal layer extending to around 750 mb. This is capped by a near-dry adiabatic lapse rate. Figure 22a (the left portion) exemplifies this configuration.

3. Theoretical Background

A. Destabilization

Mathematically, the processes in the atmosphere that lead to a change in the lapse rate at a station have been described by Johannessen (AWSM 105-124, 1969). Denoting the lapse rate by:

$$\gamma = - \partial T / \partial z$$

where T is temperature and z is height above ground.

$$\partial\gamma / \partial t = \begin{cases} \text{increasing stability} < 0 \\ \text{decreasing stability} > 0 \end{cases}$$

$$= -1/c_p \; \partial/\partial z \; (dQ / dt) \quad \{ \text{differential heating in the vertical}$$

$$- \underline{V} \cdot \nabla\gamma \quad \{ \text{advection of air of different stability}$$

$$+ \partial \underline{V} / \partial z \cdot \nabla T \quad \{ \text{shearing advection of different temperature}$$

$$+ \partial w / \partial z \; (\Gamma - \gamma) \quad \{ \text{shrinking and stretching of column}$$

$$- w \; \partial\gamma / \partial z \quad \{ \text{vertical advection of lapse rate}$$

$\underline{V}$ is the horizontal wind vector, w is vertical motion, c_p is the specific heat at constant pressure, and Q is diabatic heating.

Q indicates heat transfers by radiation and turbulence, and the latent heat exchanged during condensation and evaporation. If Q includes latent heat, Γ

must be interpreted as the saturation adiabatic lapse rate during the condensation phase, but as the dry adiabatic lapse rate otherwise. Thus, the first term in the equation for lapse rate changes can be expanded:

$$\partial\gamma/\partial t = - 1 / c_p \quad \partial/\partial z \ [d /dt \ (Q_L + Q_R + Q_T)] \ldots$$

where Q_L is latent heat exchange, and Q_R and Q_T are heat transfers by radiation and turbulence, respectively.

If there is a positive turbulent heat transfer with time and the transfer is downward then, neglecting the other terms, $\partial\gamma/\partial z > 0$ and there is decreasing stability. In a stable atmosphere the flow of heat due to turbulent eddy motion is downward, and that the ultimate effect of mixing is to produce an atmosphere with constant lapse rate equal to the adiabatic value (Sutton, 1951). Radiational cooling of cloud top layers at night and/or the release of latent heat in lower levels will cause destabilization also.

The horizontal advection of less stable air into an area will cause destabilization. If during cold air advection, the ageostrophic component to the wind increases with height, the shearing advection of different temperatures into an area will destabilize the air mass. The ageostrophic wind component consists of a local or isallobaric contribution, a downwind or advective contribution, and a contribution due to vertical advection of the wind shear (Haltiner and Martin, 1957). Since vertical shear is present during scouring episodes, an ageostrophic wind component exists to provide destabilization by cooling the air more rapidly aloft than at lower levels.

In a stretching air column the top ascends faster and will cool more rapidly than the bottom and result in less stability. Finally, the vertical advection of lapse rate will act to destabilize the air when there is net upward vertical motion in an air mass where the stability increases with height. This most likely occurs along a cold frontal surface as it moved through the Wind River Basin. Later we will find another mechanism which can generate instability as strong upward vertical motions spread numerically smaller lapse rates upward causing decreasing stability.

B. Dynamic Instability

Browning, Harrold and Starr (1970) noted that the most likely mechanism for the breakdown of stably stratified layers in the free atmosphere is dynamic, or Kelvin-Helmholtz, instability. The vertical shear of the horizontal wind is a source of dynamic instability. Although it is generally not strong enough to overcome static stability, dynamic instability often leads to turbulence (Lilly, 1986). The Richardson Number (Ri), a non-dimensional number which represents the ratio of the thermal stability to the vertical shear of the mean wind, separates stable from unstable shear-flow regimes (Hess, 1959). The more stable the lapse rate, the more turbulence is suppressed--the larger the numerator, the bigger Ri. The larger the vertical shear, the greater the tendency for turbulent eddies to form--the larger the denominator, the smaller the Ri. L. F. Richardson interpreted the ratio as the work done against gravitational stability to the energy transformed from mean to turbulent motion (Huschke, 1959).

A Ri less than 0.25 is a prerequisite for unstable flow and turbulence (Hooke, 1986). The gradient form of the Richardson Number is:

$$Ri = g/\Theta \; d\Theta/dz \; / \; (dU/dz)^2 \qquad \text{(Hooke, 1986)}$$

or as used here:

$$Ri = g \; d\ln\Theta/dz \; / \; (du/dz)^2 + (dv/dz)^2$$

where g = gravitational acceleration, Θ = potential temperature, U is the wind speed, and (u,v) are the (x,y) components of the mean horizontal wind.

We also calculate a Richardson Number for the moist atmosphere defined as:

$$Rie = g \; d\ln\Theta_e/dz \; / \; (du/dz)^2 + (dv/dz)^2$$

where Θ_e = equivalent potential temperature.

$$\Theta_e \tilde{=} \Theta \exp \; (L_c \; q_s \; / \; c_p \; T) \qquad \text{(Holton, 1979)}$$

L_c is latent heat of condensation, q_s is saturation mixing ratio, and T is temperature. This is a slight variation of the moist Richardson Number defined by Browning, Harrold and Starr (1970) which utilized wet bulb potential temperature.

It is difficult to test or utilize for prediction the 0.25 critical Richardson Number because criterion need only be exceeded over only a small region for a short period. The Ri itself is a notoriously unstable statistic whose value depends on the scale over which it is measured (Reiter and Lester, 1967). The Ri is highly variable in space and frequently ranges from zero to $\pm$ infinity (Lilly, 1986). To compute Ri, the vertical resolution of the observations must be less than the depth over which turbulent breakdown occurs. Routine radiosonde ascents usually do not provide sufficient detail or representativity (Browning, Harrold and Starr, 1970). However, there is observational evidence that in strong frontal zones the Ri is about 0.25 (Ludlam, 1967).

In summary, scouring events occur only with the eastward passage of a strong cold front. Because of the height of the terrain (Fig. 1) west through northeast of the Wind River Basin, low to mid-level portions of Pacific or Canadian cold fronts have to re-form after crossing the mountains. The formation of a mid-tropospheric front increases the vertical wind shear and lowers the Ri (Shapiro, 1974). Amplifying gravity waves in this shear flow further aid in the destabilization.

4. Case Studies

A. November 15, 1986--Inversion Break

On November 11th and 12th a Canadian air mass dropped southeastward out of Alberta on the anticyclonic side of an upper tropospheric trough rotating

around an upper low near Hudson's Bay (Figs. 2 and 3). The Canadian air mass settled over the Wind River Basin. The high temperatures at Lander were 18 and 19°F on the 12th and 13th, respectively, having cooled from the 40°F high on the 11th. The lows on the 12th and 13th were -1 and -4°F. The snow depth was four inches from the 12th through 14th, although it decreased to three inches by the 12 UTC November 15th observation.

On the morning of the 14th, as an upper trough extending west-southwestward from the Hudson Bay low was moving into the Pacific Northwest, another mass of cold Canadian air was dropping south along the northern Rockies (Figs. 4 and 5). However, a Pacific cold front was also moving inland. By 12 UTC on the 15th, the Canadian air mass had backed into the Wind River Basin. The remains of the Pacific front, and the upper level trough were just upstream of the Basin (Figs. 6 and 7). These combined systems scoured the cold air from the Basin. Figure 8 shows a 10°F warming from 09 UTC to 12 UTC on the 15th associated with a wind shift to the east and significant dew point temperature rise as the new Canadian air mass replaced the old one which had stagnated in the Basin.

The soundings during this episode are shown in Figure 9. At 12 UTC November 14th there was a very strong radiation inversion (temperature increase rate of 95°C km^{-1}) off the surface capped by the remains of a subsidence inversion. During the next 12 hours, the wind directions below the 500 mb level became westerly as speeds generally increased. Altocumulus standing lenticular (ACSL) clouds, evidence of increasing winds, shear aloft, and dynamic destabilization, were observed much of the period (Fig. 8). The slope of the Θ surfaces from the 14th at 12 UTC to 00 UTC on the 15th between 700 mb down and the top of the inversion indicate warming during that period (Fig. 10). The surface pressure at 00 UTC was 807 mb, having decreased from 814 mb at 12 UTC November 14th. This also indicates that a net warming of the air column above Lander had occurred.

On the 00 UTC sounding the Ri numbers in the two 1,000 feet layers immediately above and below 700 mb were below 0.25 (Fig. 9b). Since the top of the Wind River Range immediately upstream of the Basin is slightly higher than the 700 mb level, it provides a strong mechanical disturbance to air flowing into the Basin. This is believed to be the reason the initial unstable layers appear near 700 mb. Hooke (1986) noted that air flow over mountainous terrain is a persistent forcing mechanism capable of generating gravity waves. Figures 10a, 10b, and 11b show a slight increase in Θ values in the layers bounding 700 mb with wind shear values varying from 18.1 to 18.6 m sec^{-1} km^{-1}. This amounts to about 10 kts of speed increase per 1,000 feet through the unstable layers. Further, in the unstable layers, the west wind component is an order of magnitude greater than the north or south component. This consistency of the wind direction is significant in light of the topographical features immediately upstream of the Basin. At 00 UTC the temperature increase rate off the surface was 45.8°C km^{-1}, a decrease of over half the previous (12 UTC) value.

The 00 UTC November 15th sounding possesses many of the characteristics typically present just before inversion break: strong generally west winds at mountain top level (near 700 mb or 4,000 to 6,000 feet AGL); and Ri values less than 0.25 just above or below 700 mb with vertical shear in those unstable

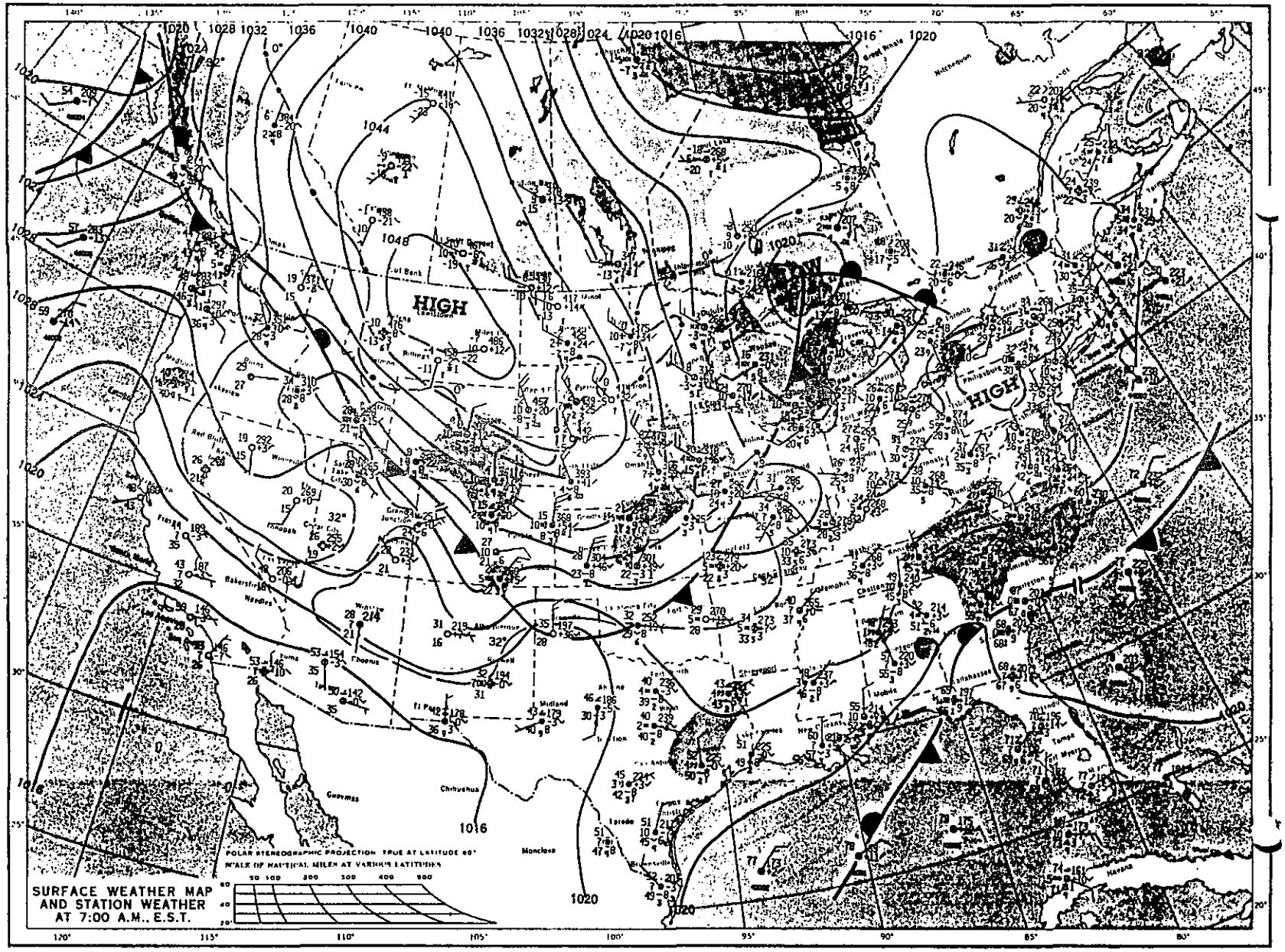

Fig. 2. Surface/sea level pressure analysis for 12 UTC November 12, 1986.

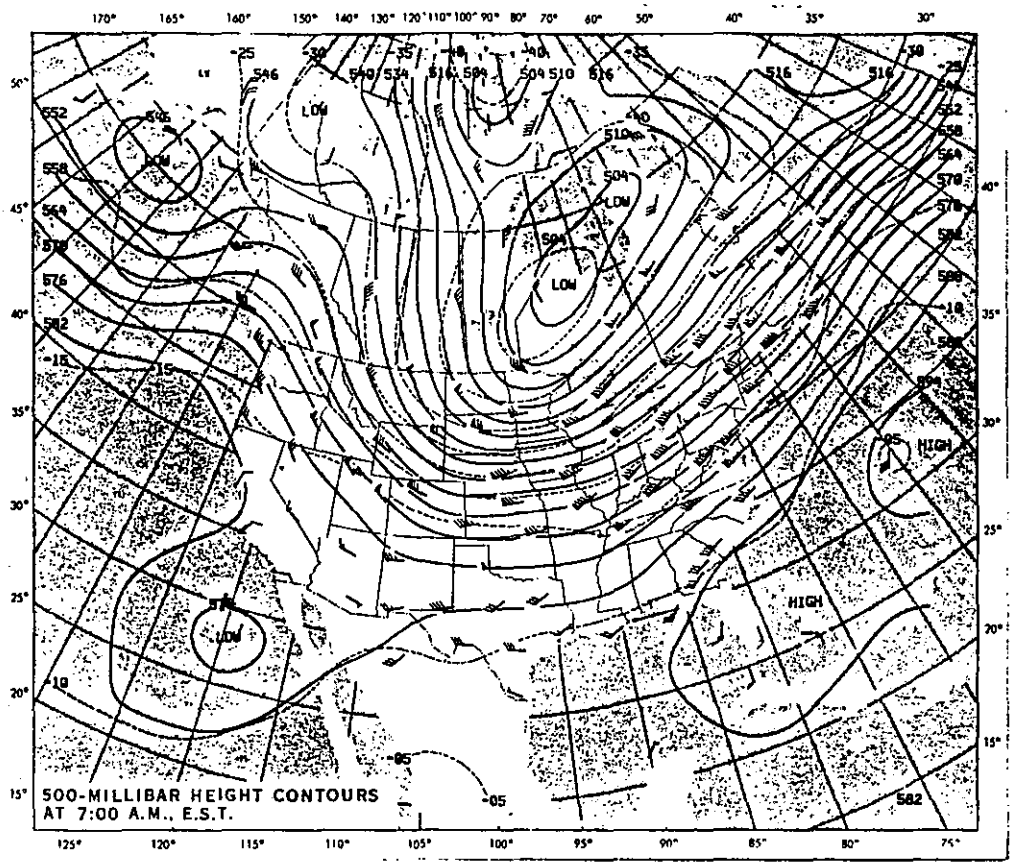

Fig. 3. 500 mb Chart for 12 UTC November 12, 1986.

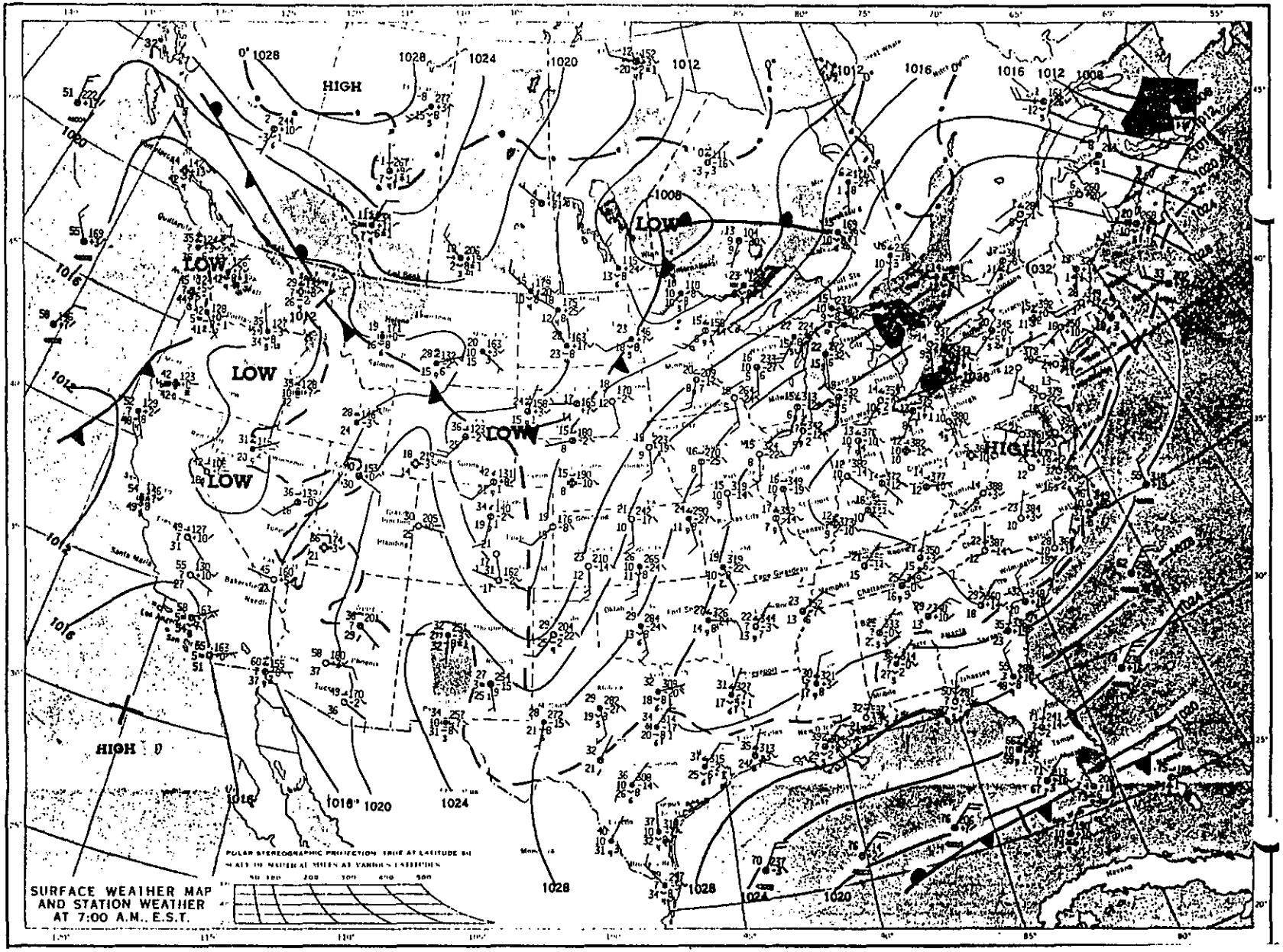

Fig. 4. Surface/sea level pressure analysis for 12 UTC November 14, 1986.

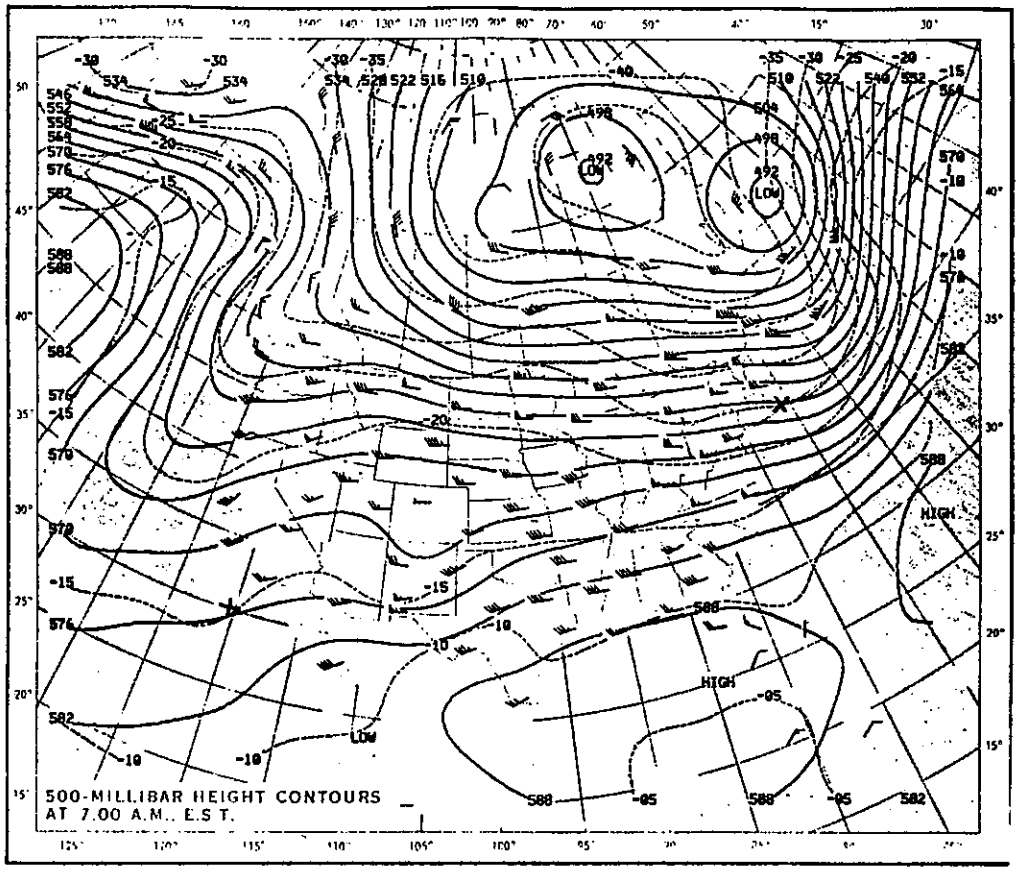

Fig. 5. 500 mb Chart for 12 UTC November 14, 1986.

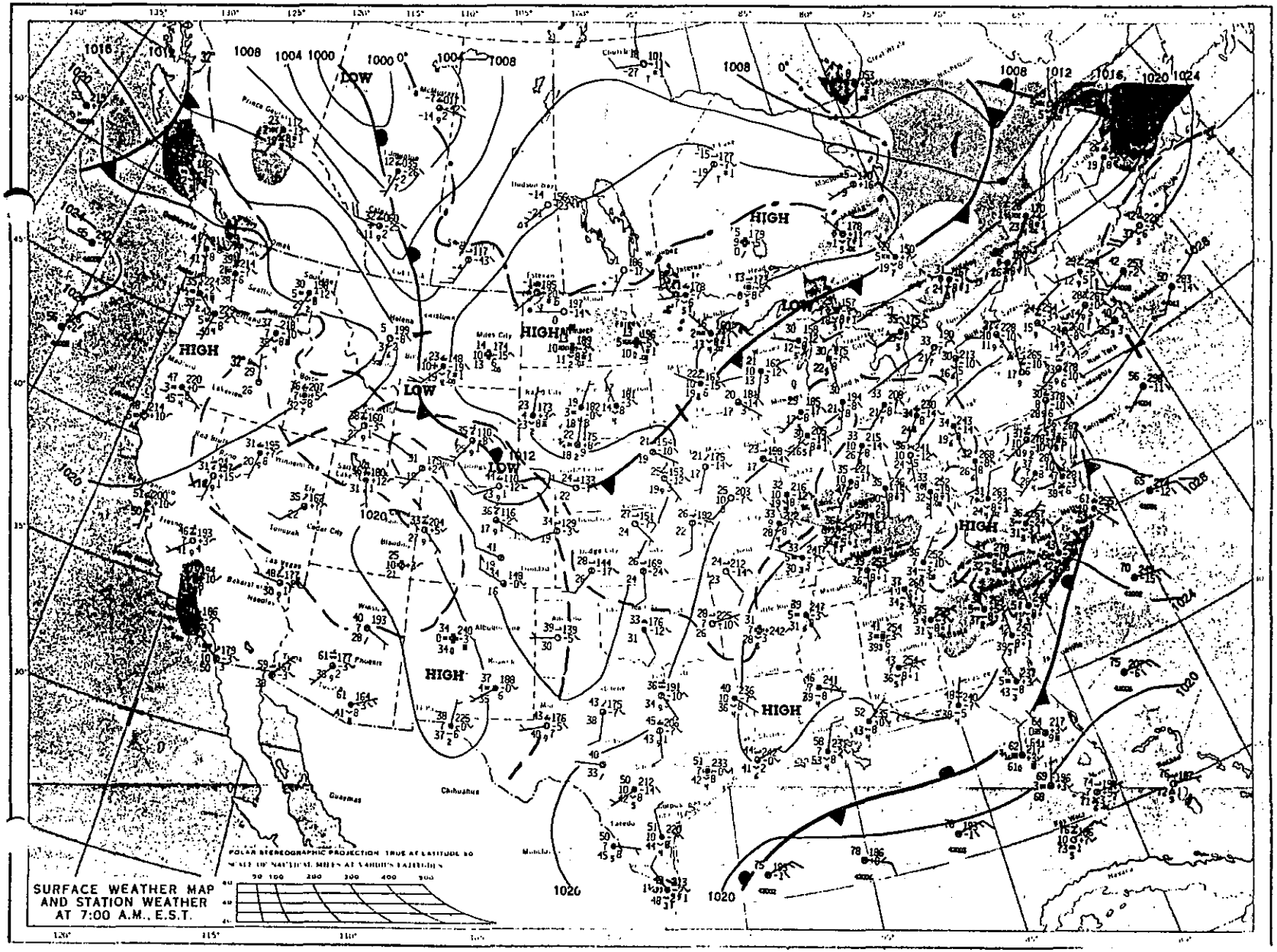

Fig. 6. Surface/sea level pressure analysis for 12 UTC November 15, 1986.

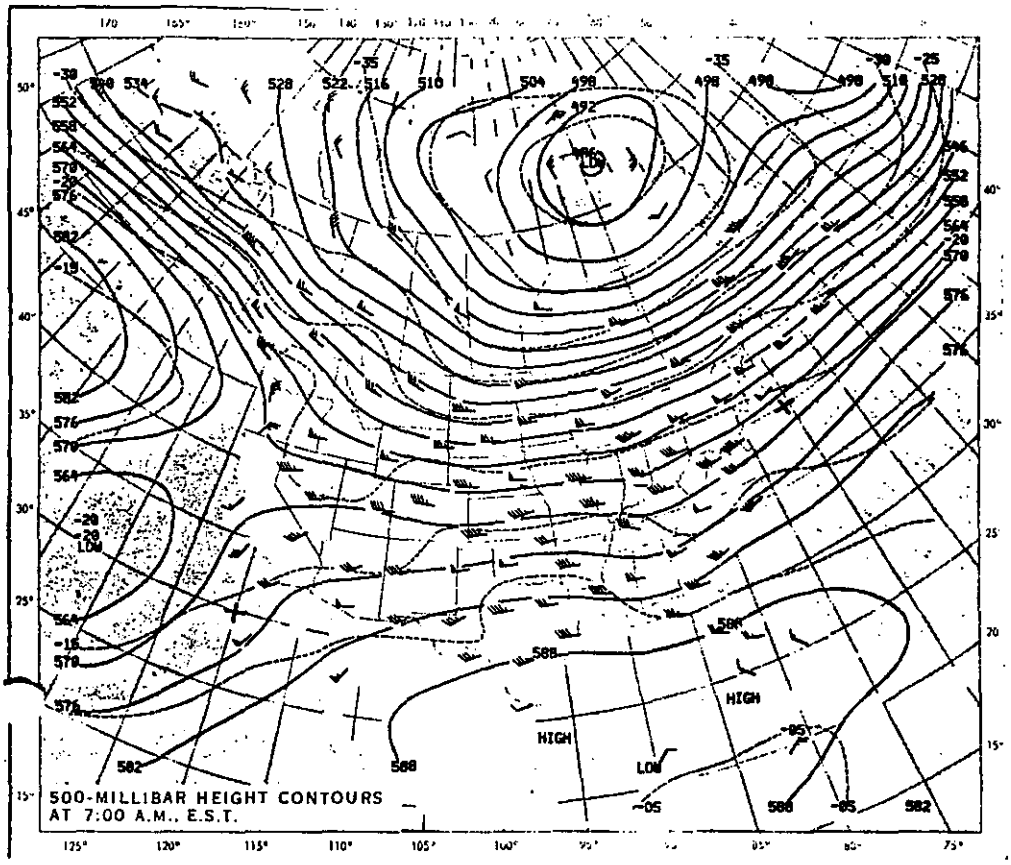

Fig. 7. 500 mb Chart for 12 UTC November 15, 1986.

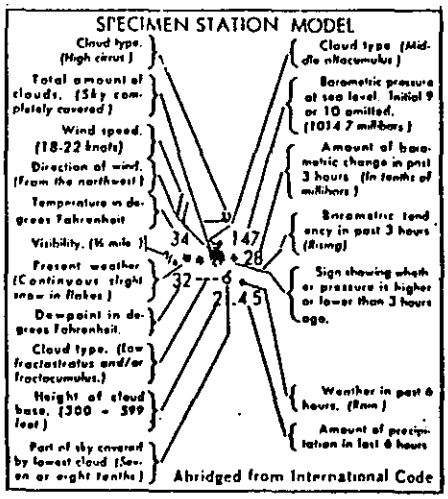

10
9
021
00^
8/10 Cs
14/12Z

14
(*)
022
07/
12
2/10 ACSL 7/10 CS
15Z

25
(*)
020
02✓
21
2
1/10 ACSL 9/10 CS
18Z

31
(*)
018
-14L
26
1/10 ACSL 9/10 CS
21Z

28
018
02✓
25
1/10 CU 1/10 ACSL 8/10 CS
15/00Z

27
018
03[
24
8
1/10 Sc 6/10 CS
03Z

28
017
02^
4
24
2/10 ACSL 7/10 Cs
06Z

31
015
-05L
26
3/10 Cs
09Z

41
013
-03L
33
½
FEW Sc, Ac 4/10 Cs
15/12Z

Fig. 8. Surface weather plot for Lander at three hour intervals from 12 UTC November 14 to 12 UTC November 15, 1986. Cloud amounts and types a... to lower right of plot.

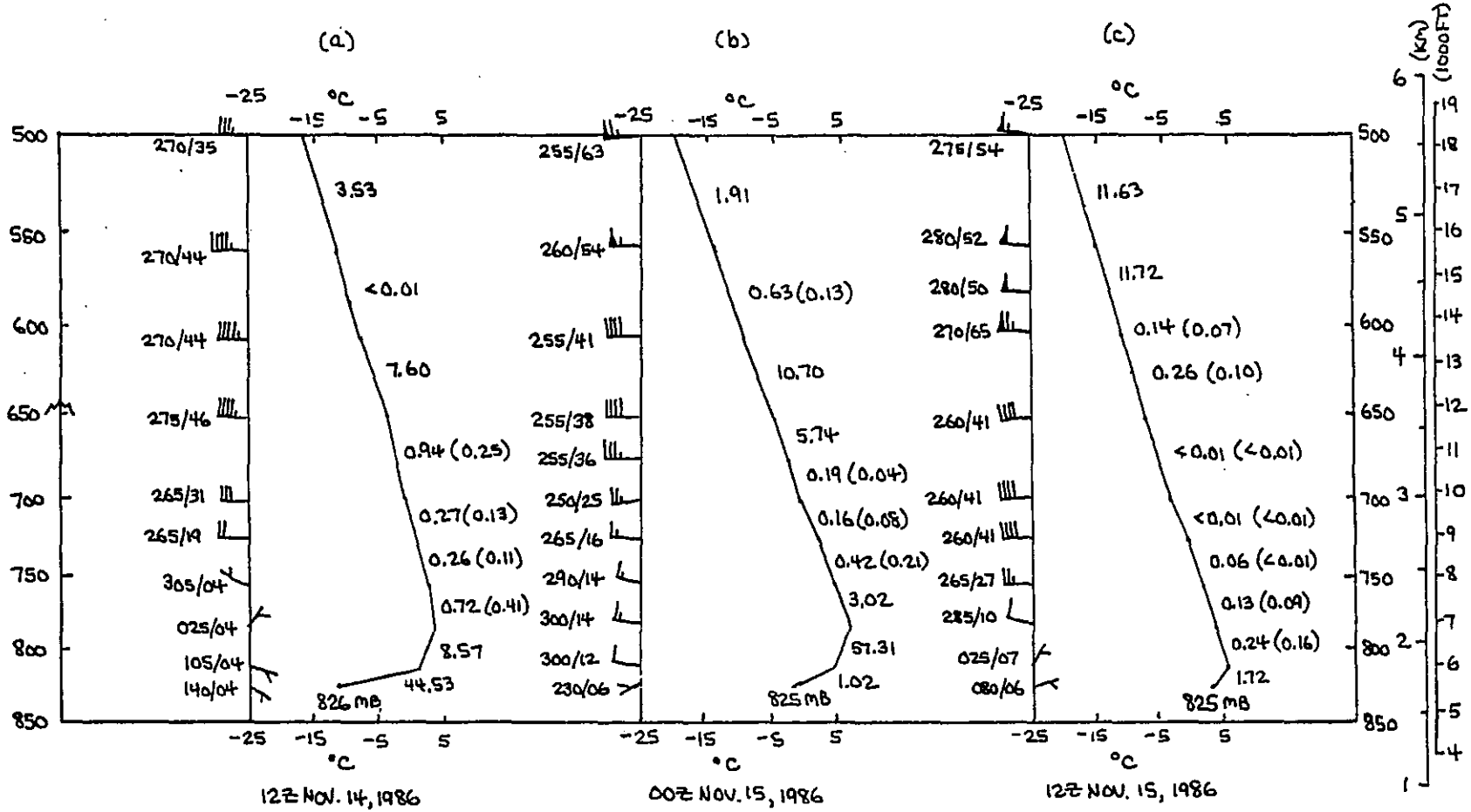

Fig. 9. Time-height variation of temperature (°C) and wind (DEG and kts) at Lander from surface to 500 mb for 12 UTC November 14, 00 UTC November 15 and 12 UTC November 15, 1986. Richardson numbers are to right of each temperature curve, and selected moist Richardson numbers are to the right of those in parentheses.

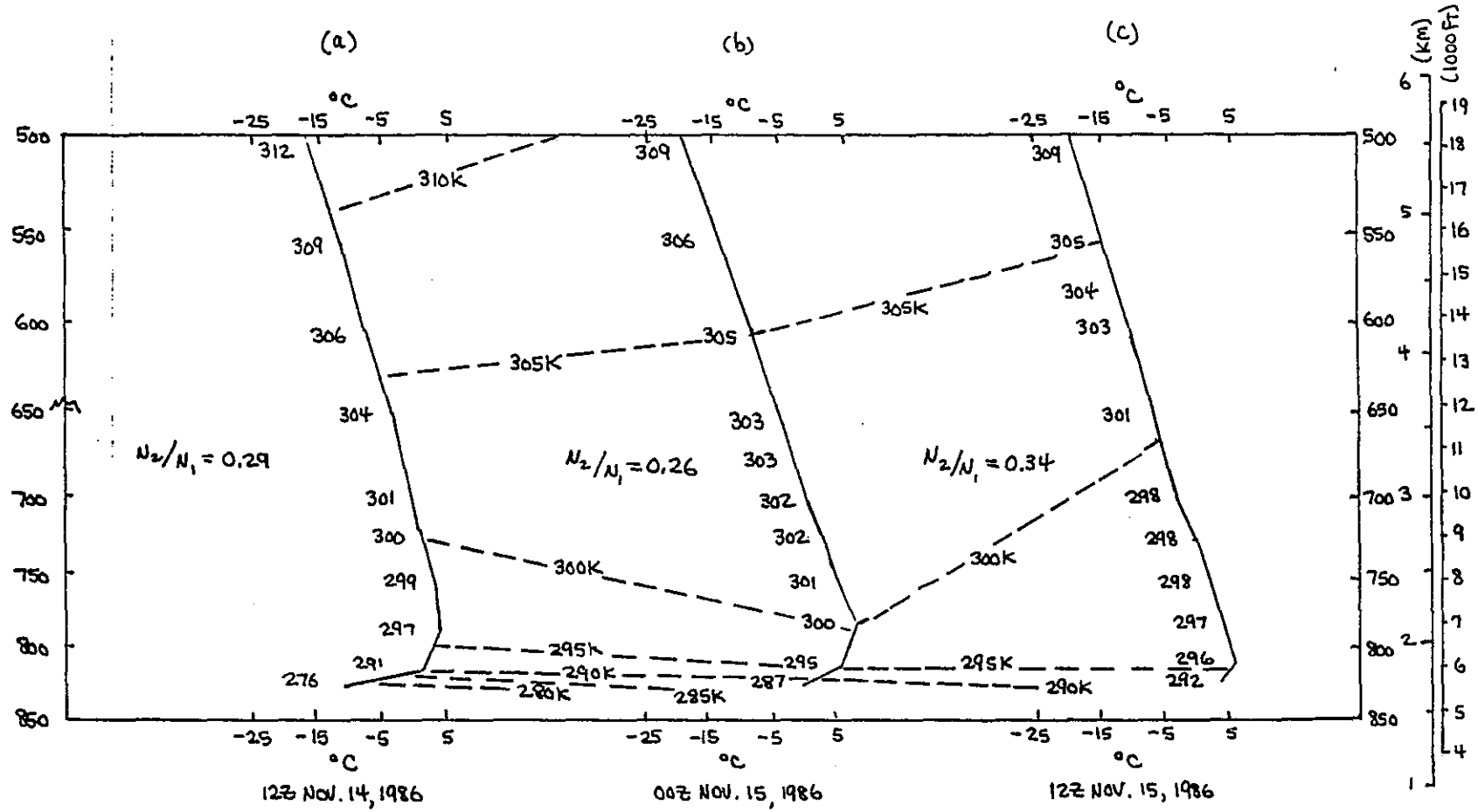

Fig. 10. Time-height variation of temperature (°C) at Lander from surface to 500 mb for 12 UTC November 14, 00 UTC November 15 and 12 UTC November 15, 1986. Potential temperatures (°K) are to left of each temperature curve.

layers of greater than 15 m sec^{-1} km^{-1}, (about 10 kts per 1,000 feet). There is generally a temperature increase rate immediately off the surface of around 40°C km^{-1} or more on both of the last two soundings before inversion break.

Figure 11 shows increasing lapse rates between 12 UTC on November 14th to 00 UTC on November 15th from the inversion up to 500 mb. While part of this destabilization was most likely the result of the horizontal advection of lapse rates ahead of the approaching disturbance, with the strong wind shear present, shearing advection of different temperatures was also destabilizing the air mass. The daytime heating cycle was also destabilizing the air mass by radiational heat transfer. By 00 UTC a layer straddling 700 mb had become dynamically unstable and the ensuing turbulent heat transfer began further reducing the static stability.

At 12 UTC on the 15th, following inversion break, lapse rates were decreasing through the mid and upper levels of the air mass (above 700 mb) following the frontal passage and indicating destabilization processes had been reversed. The low Ri values at 12 UTC showed dynamic instability was still present (Fig. 9c).

Figure 10 shows that by 12 UTC on the 15th the Θ gradient in the lowest several thousand feet decreased by a factor of three. This decrease in static stability was due to turbulent energy transfer as well as the changed air mass. The colder Θ values at each level, with respect to the previous sounding (Figs. 10b and c), indicated the passage of a surface to 500 mb cold frontal boundary.

Figure 9 has moist Richardson numbers (Rie) in parentheses to the right of the Ri values, whenever the Ri is less than 0.7. Note that the Rie values are smaller. This agrees with Einaudi and Lalas (1973), who found that in an atmosphere with shear, condensation tends to make the atmosphere less dynamically stable. The same amount of vertical wind shear will produce a lower Richardson number (and thus more turbulence) in a moist atmosphere than in a dry one.

B. December 30, 1986--Inversion Break

Figures 12 and 13 show a surface to 500 mb pressure ridge in western of Wyoming at 12 UTC December 29, 1986. Figure 14a indicates stable Ri values through the depth of the sounding. The rate of temperature increase off the surface was 67.7°C km^{-1} (Fig. 16a). Wind speeds were light from the surface to 700 mb with considerable variation in direction. The snow depth at Lander had been five inches for several weeks. For several days prior to the 29th, temperatures had been relatively constant with highs around 30°F and lows from 5 to 13°F.

By 00 UTC December 30 westerly winds had developed throughout the sounding. The layer just above 700 mb had its Ri decrease to 0.19 (Fig. 14b) and had 20.8 m sec^{-1} km^{-1} of vertical shear (9 kts through the 1,000 feet layer) (Fig. 16b). ACSL clouds were observed at 21 UTC (Fig. 17), a hint of the instability which would be shown on the sounding several hours later. Above the inversion, descent of the Θ surfaces from 12 UTC to 00 UTC indicated warming (Figs. 15a and b). Also, the surface pressure fell from 836 mb at 12 UTC to 833 mb at 00 UTC, and 831 mb at 12 UTC December 30th.

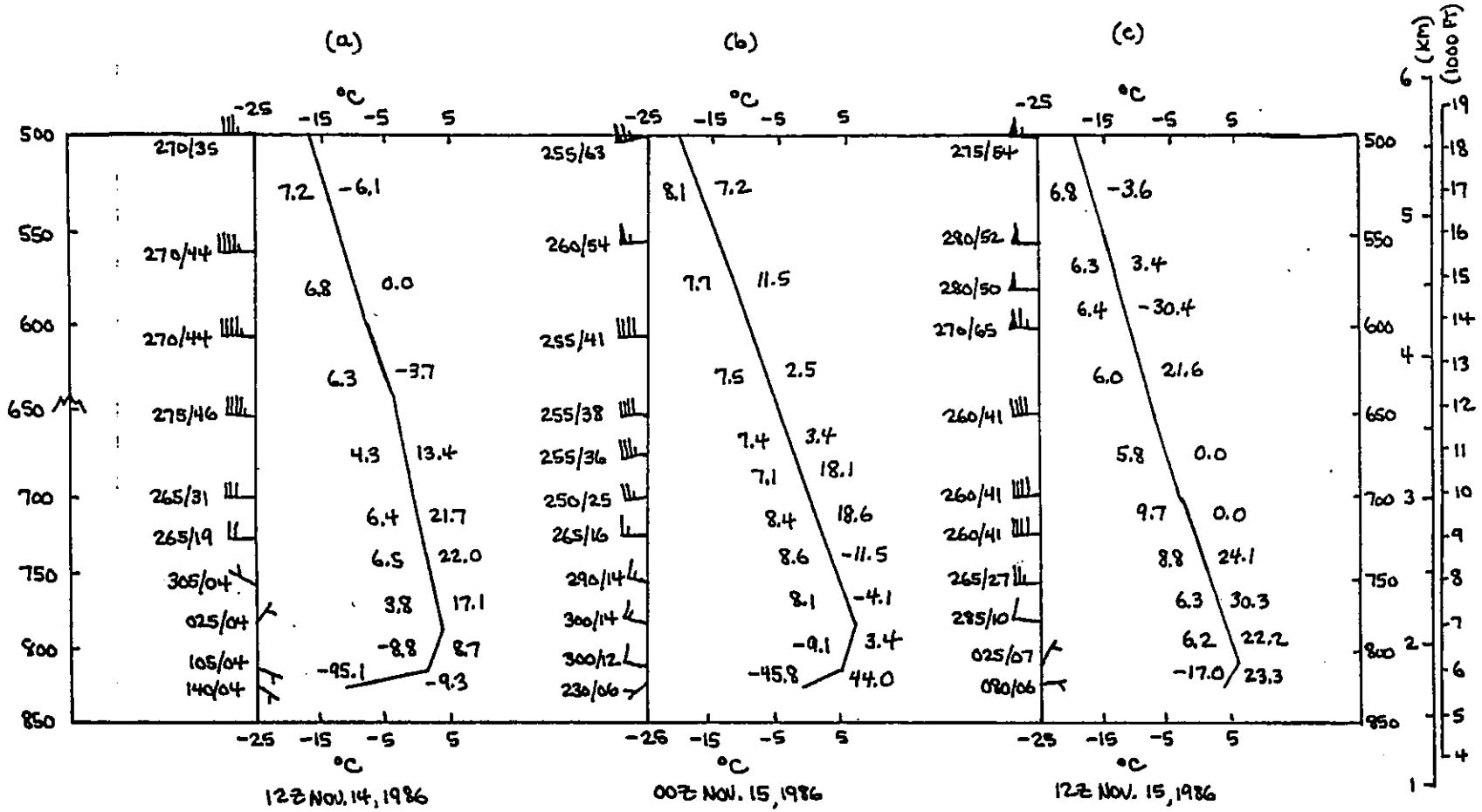

Fig. 11. Time-height variation of temperature (°C) and wind (DEG and kts) at Lander from surface to 500 mb for 12 UTC November 14, 00 UTC November 15 and 12 UTC November 15, 1986. Lapse rates (°C km^{-1}) are to the left of each temperature curve, and wind shear values (m sec^{-1} km^{-1}) to the right.

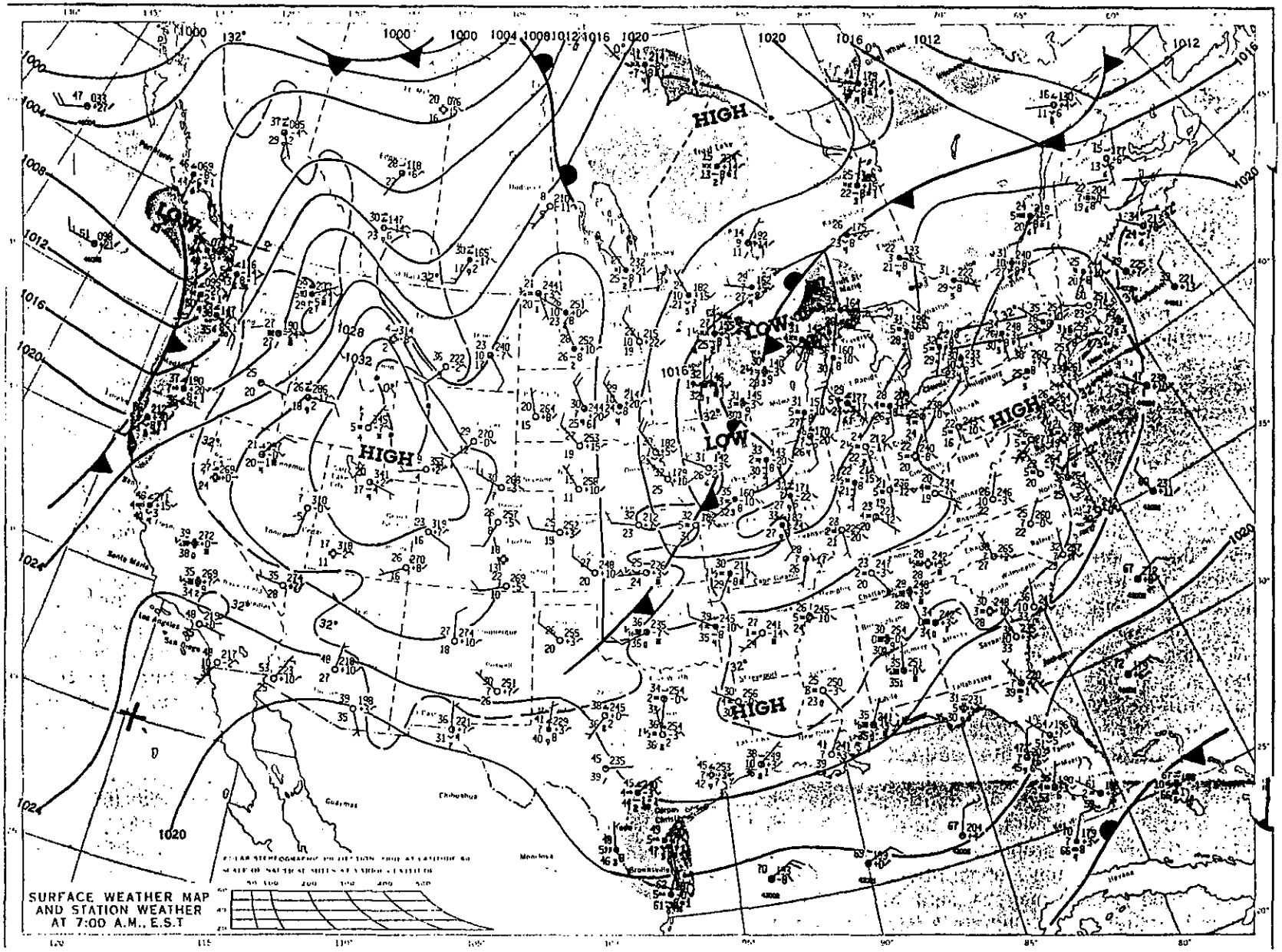

Fig. 12. Surface/sea level pressure analysis for 12 UTC December 29, 1986.

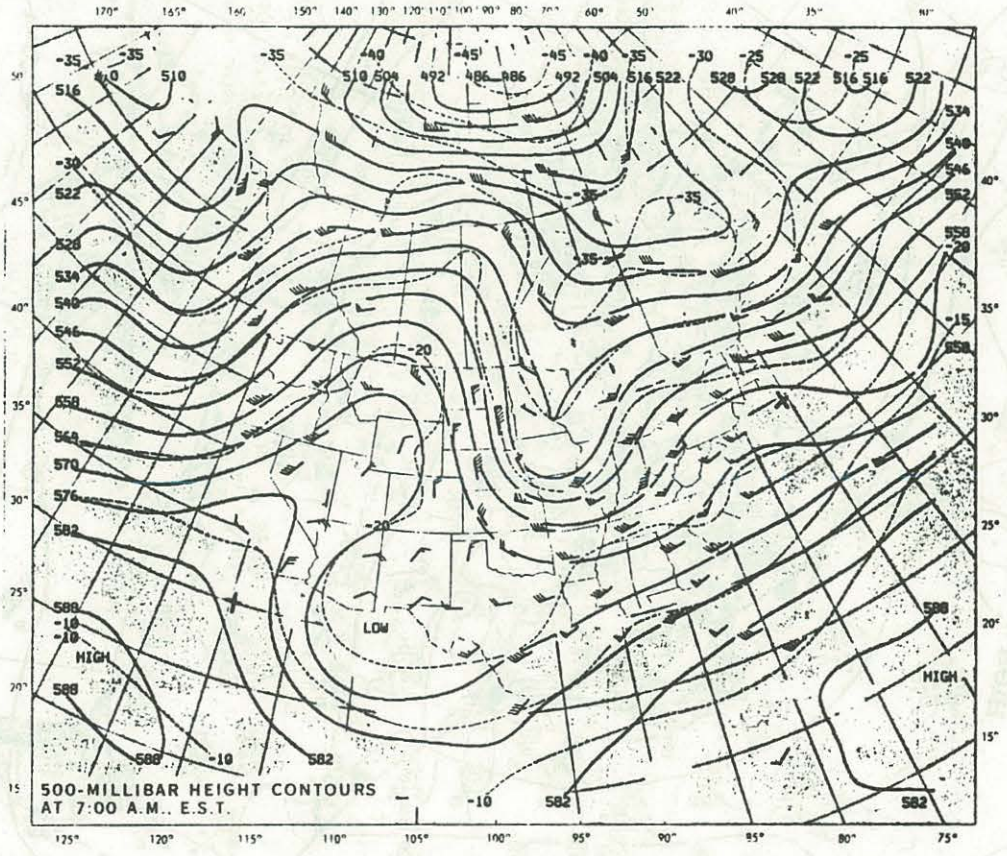

Fig. 13. 500 mb Chart for 12 UTC December 29, 1986.

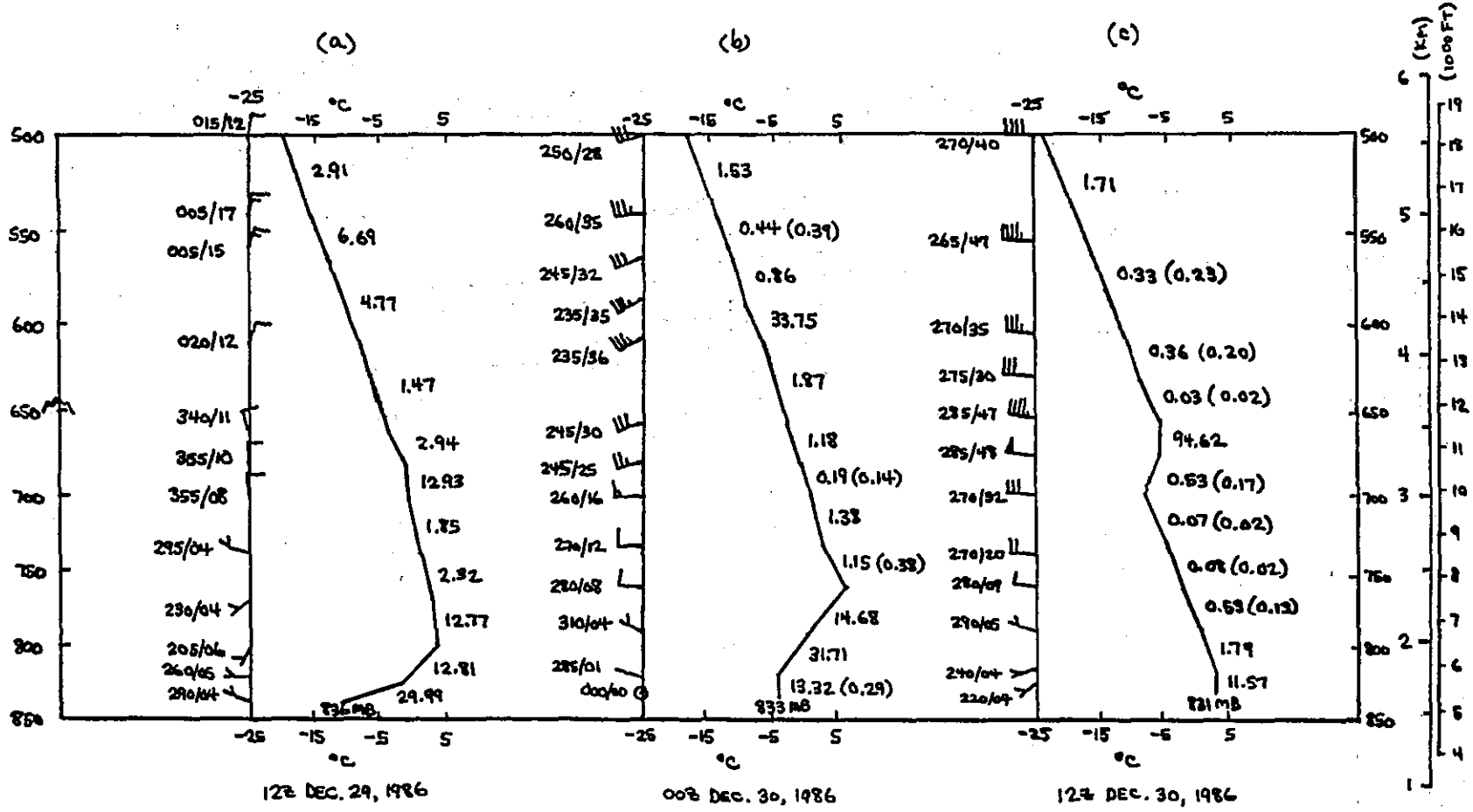

Fig. 14. Time-height variation of temperature (°C) and wind (DEG and kts) at Lander from surface to 500 mb for 12 UTC December 29, 00 UTC December 30, and 12 UTC December 30, 1986. Richardson numbers are to right of each temperature curve, and selected moist Richardson numbers are to the right of those in parentheses.

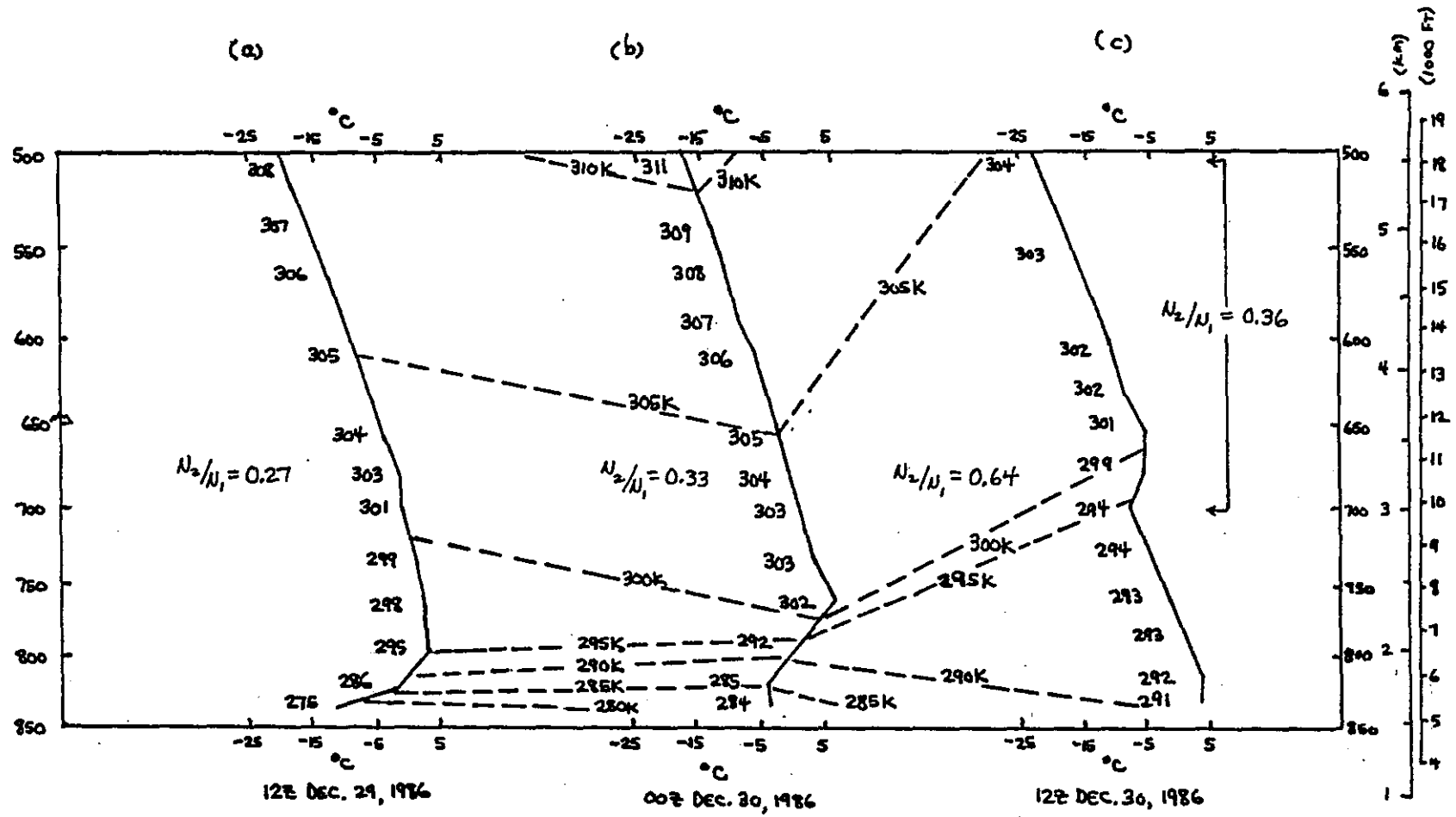

Fig. 15. Time-height variation of temperature (°C) at Lander from surface to 500 mb for 12 UTC December 29, 00 UTC December 30, and 12 UTC December 30, 1986. Potential temperatures (°K) are to left of each temperature curve.

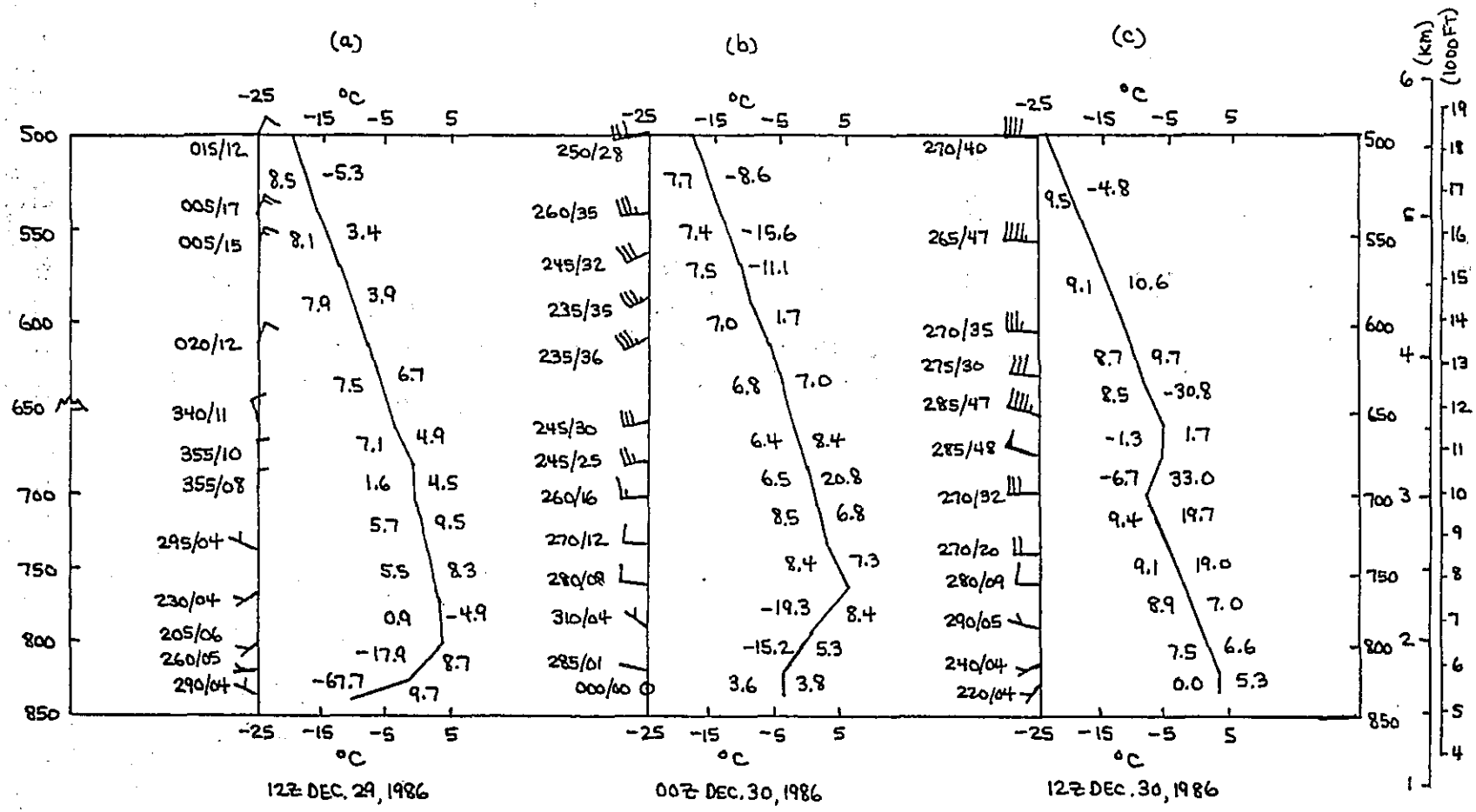

Fig. 16. Time-height variation of temperature (°C) and wind (DEG and kts) at Lander from surface to 500 mb for 12 UTC December 29, 00 UTC December 30, and 12 UTC December 30, 1986. Lapse rates (°C km^{-1}) are to left of each temperature curve, and wind shear values (m sec^{-1} km^{-1}) to the right.

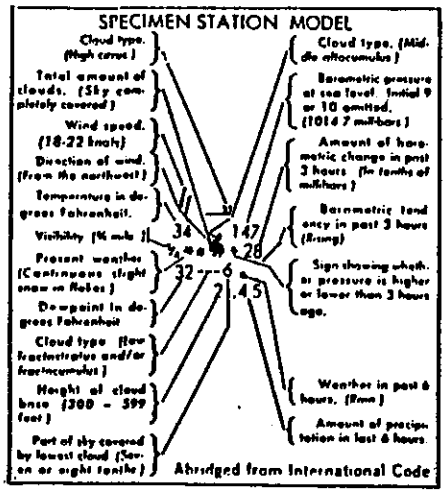

14 033 7 001
8
29/12Z

6
0 035
2 02✓
Few Cs
15Z

18
(*) 033
8 02^
6/10 Cs
18Z

24 6 029
(*) -36L
12 1/10 RCSL 9/10 Cs
21Z

22 028
13 -05^
8 6/10 Rc 4/10 Cs
30/00Z

18 028
11 -08^
5 7/10 Cs
03Z

19 026
10 -02✓
8
06Z

27
2 024
21 -02✓
2/10 Cs
09Z

5
36 022
27 -07L
5/10 Cs
30/12Z

Fig. 17. Surface weather plot for Lander at three hour intervals from 12 UTC December 29 to 12 UTC December 30, 1986. Cloud amounts and types ar to lower right of plot.

At this point the cold air was trapped in the Wind River Basin since scouring could not occur because of the lack of a mature cold front. However, Figures 18 and 19 show one approaching the northwest corner of Wyoming at 12 UTC on the 30th. One would expect this front to produce a scouring of the stagnant air from the Basin. Even though lapse rate changes from 12 UTC on the 29th to 00 UTC on the 30th were not as dramatic as in the previous case, values from the inversion to just above 700 mb were increasing (i.e., destabilization). In contrast, lapse rates were decreasing higher on the sounding. Temperatures from 700 mb to 500 mb were warming at about the same rate, resulting in neither stretching or shrinking of the column. Shearing advection of different temperatures was not significant because only vertical shear prevailed through the sounding until after 00 UTC. Thus, the changes were likely due to a combination of horizontal lapse rate advection and the radiational effect of the diurnal cycle.

Figure 17 shows the Lander surface observations from 12 UTC December 29th to 12 UTC December 30th. The changes from 06 UTC to 12 UTC—a 17°F warming of the temperature and dew point, a veering of the wind to the north or northwest—definitely indicate a break of the inversion. Further, the reversal of the slope of the θ surfaces (Fig. 15c) indicates that the cold frontal passage had occurred by 12 UTC even though the surface chart (Fig. 18) for 12 UTC still has the cold front west of the northwest corner of the state. The post-frontal sounding still indicated several dynamically unstable layers in the cold air with respect to either Ri and Rie (Fig. 14c). The inversion that is present at and just above 700 mb is probably the frontal zone aloft and is associated with a near 50 kt jet at 650 mb.

C. December 27, 1986--Inversion Failed to Break

At 12 UTC December 26, 1986, a positively tilted short wave trough extended from northern Alberta, Canada to along the Oregon coast (Fig. 20). The shearing trough shows up best in the thermal field. Figure 21 shows an associated surface trough (or weak front) along the lee side of the Rockies in southern Alberta and central Montana. The temperature profile for 12 UTC December 26th (Fig. 22a) shows the typical stagnant air mass configuration--surface-based radiation inversion capped by a subsidence inversion or near isothermal layer. Light west to northwest winds prevail from the surface to 700 mb with stable Richardson numbers. The snow depth at 12 UTC December 26th was five inches, and it remained that through 12 UTC the following day.

From 12 UTC to 00 UTC December 27th there was mid-level warming, from about 650-750 mb, with cooling at higher levels (Figs. 22, 23a and b). On Figures 23a and b the warming is reflected in lowering θ surfaces with the cooling aloft raising potential temperature surfaces. Destabilization was occurring as lapse rate values were increasing through most of the air mass during the day. Horizontal advection of lapse rate was probably having an effect as cooling aloft and stronger warming at mid-levels was observed. Also, there was the radiational effect of the diurnal cycle. Since the vertical shear was minimal, shearing advection of different temperatures was probably not significant.

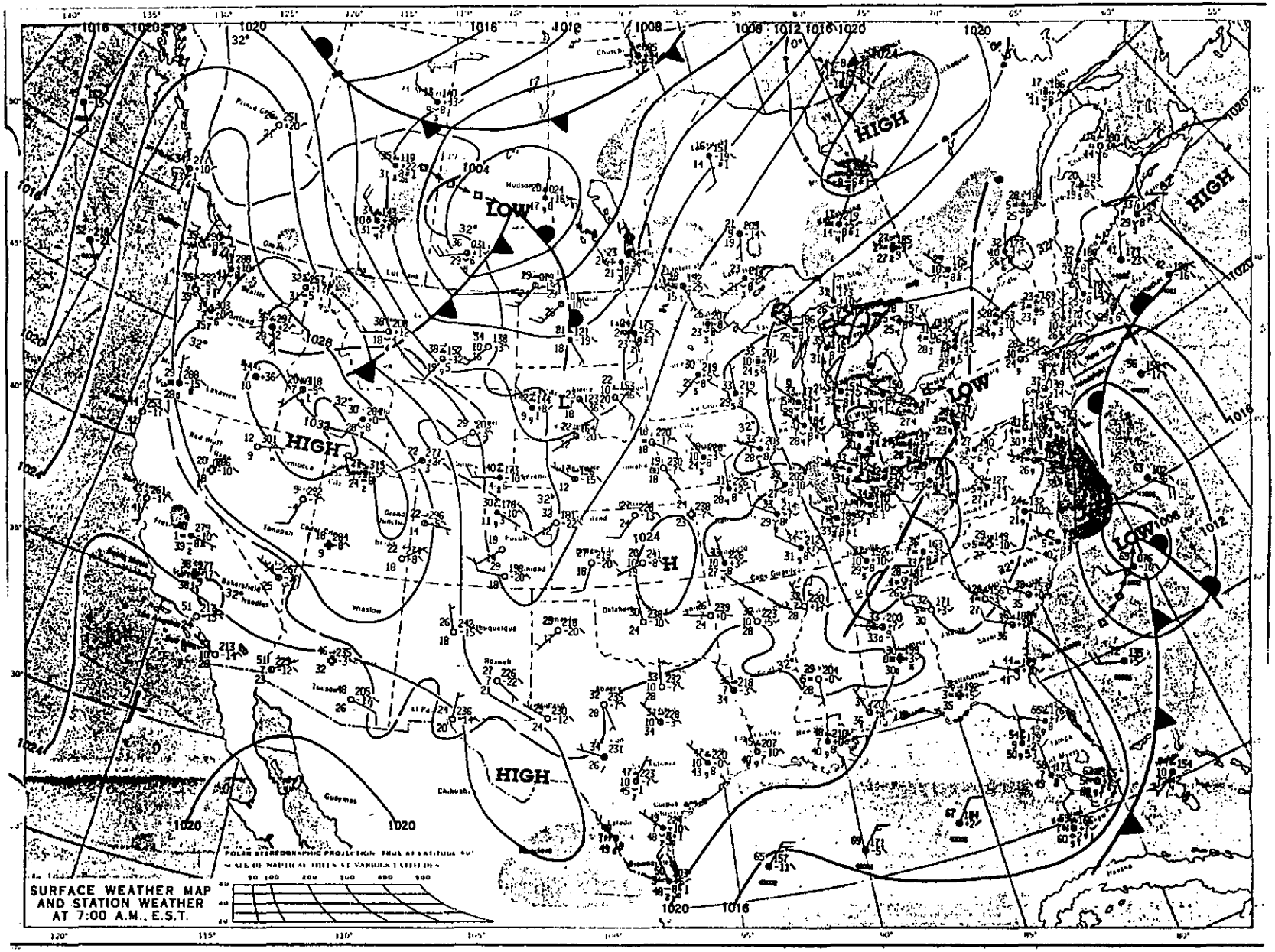

Fig. 18. Surface/sea level pressure analysis for 12 UTC December 30, 1986.

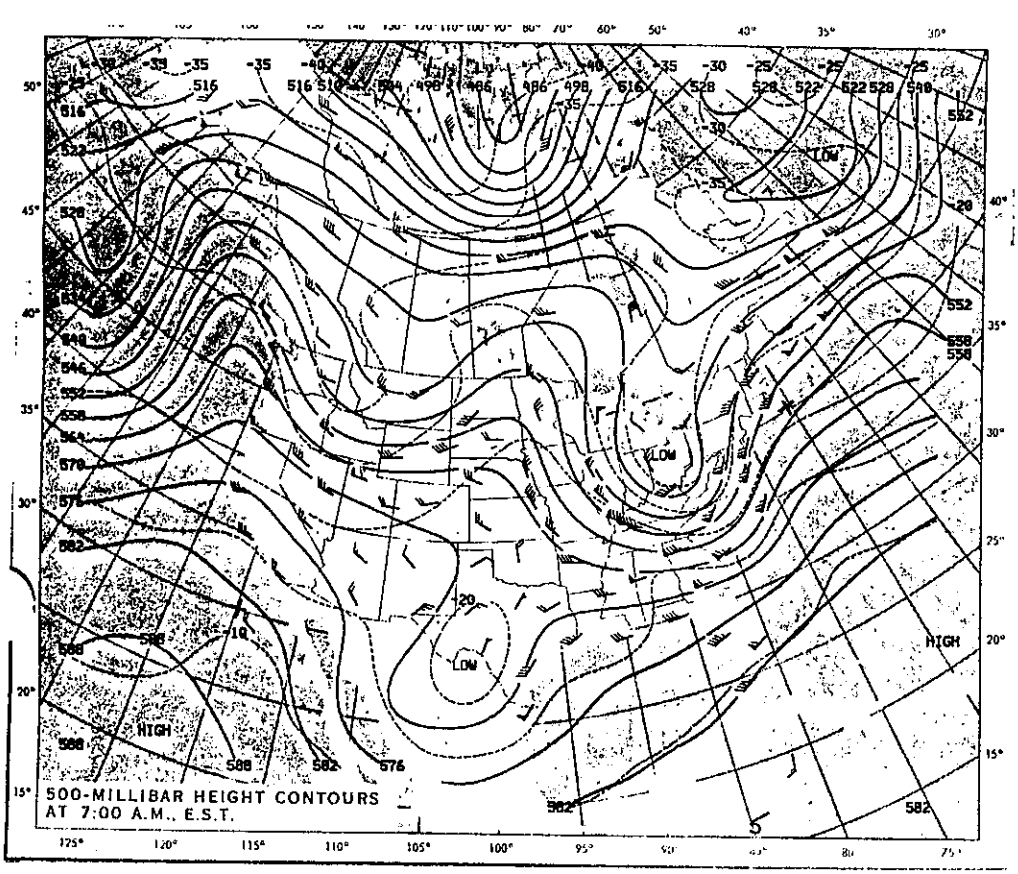

Fig. 19. 500 mb Chart for 12 UTC December 30, 1986.

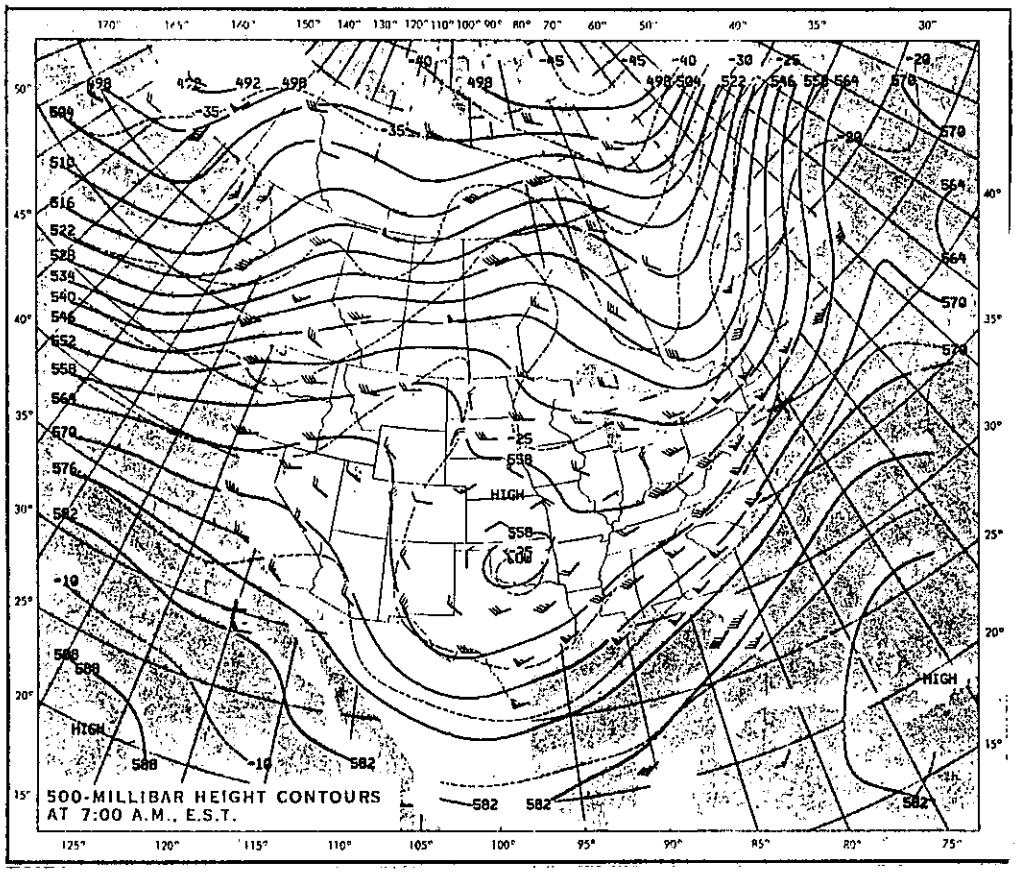

Fig. 20. 500 mb Chart for 12 UTC December 26, 1986.

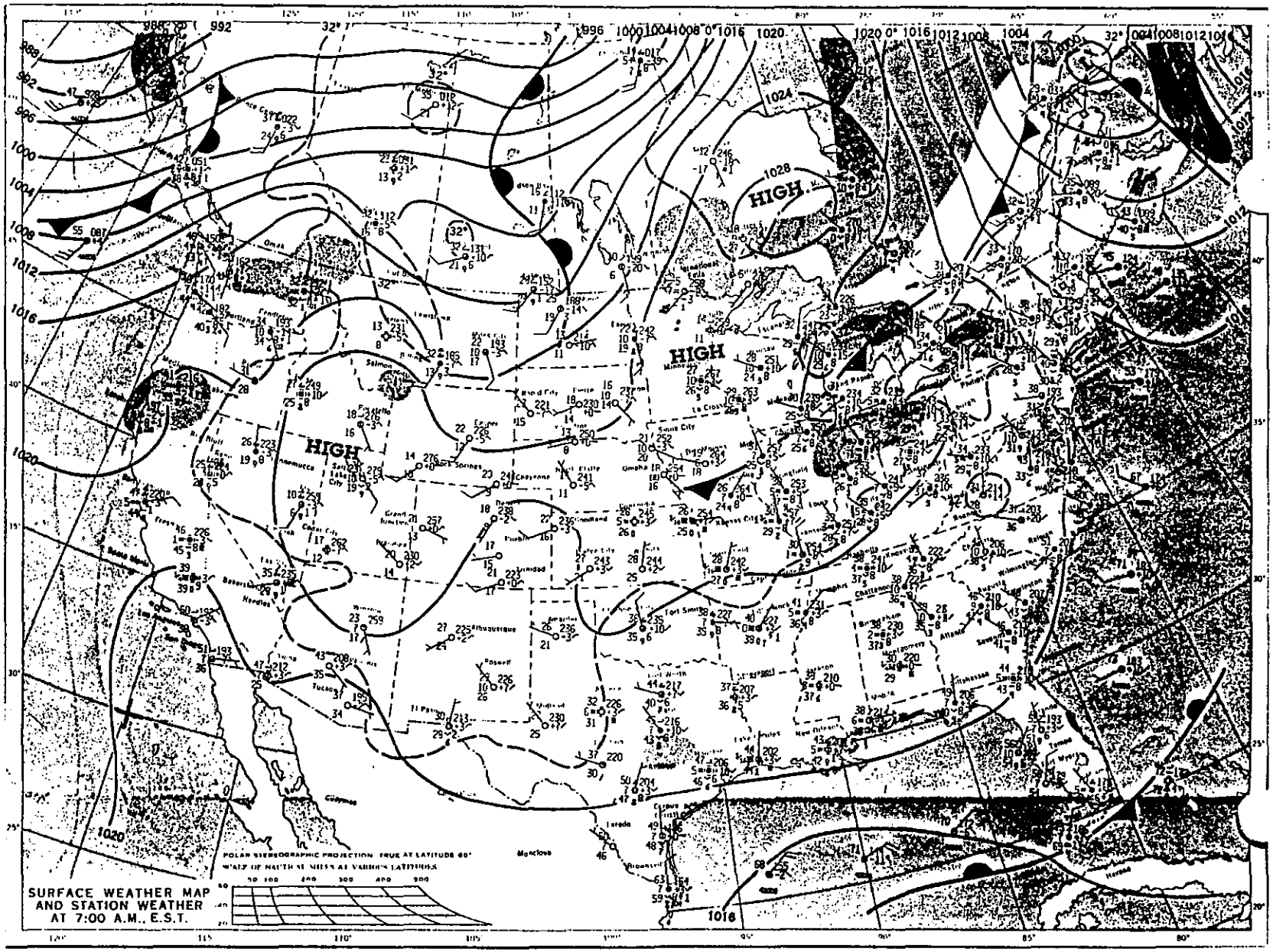

Fig. 21. Surface/sea level pressure analysis for 12 UTC December 26, 1986.

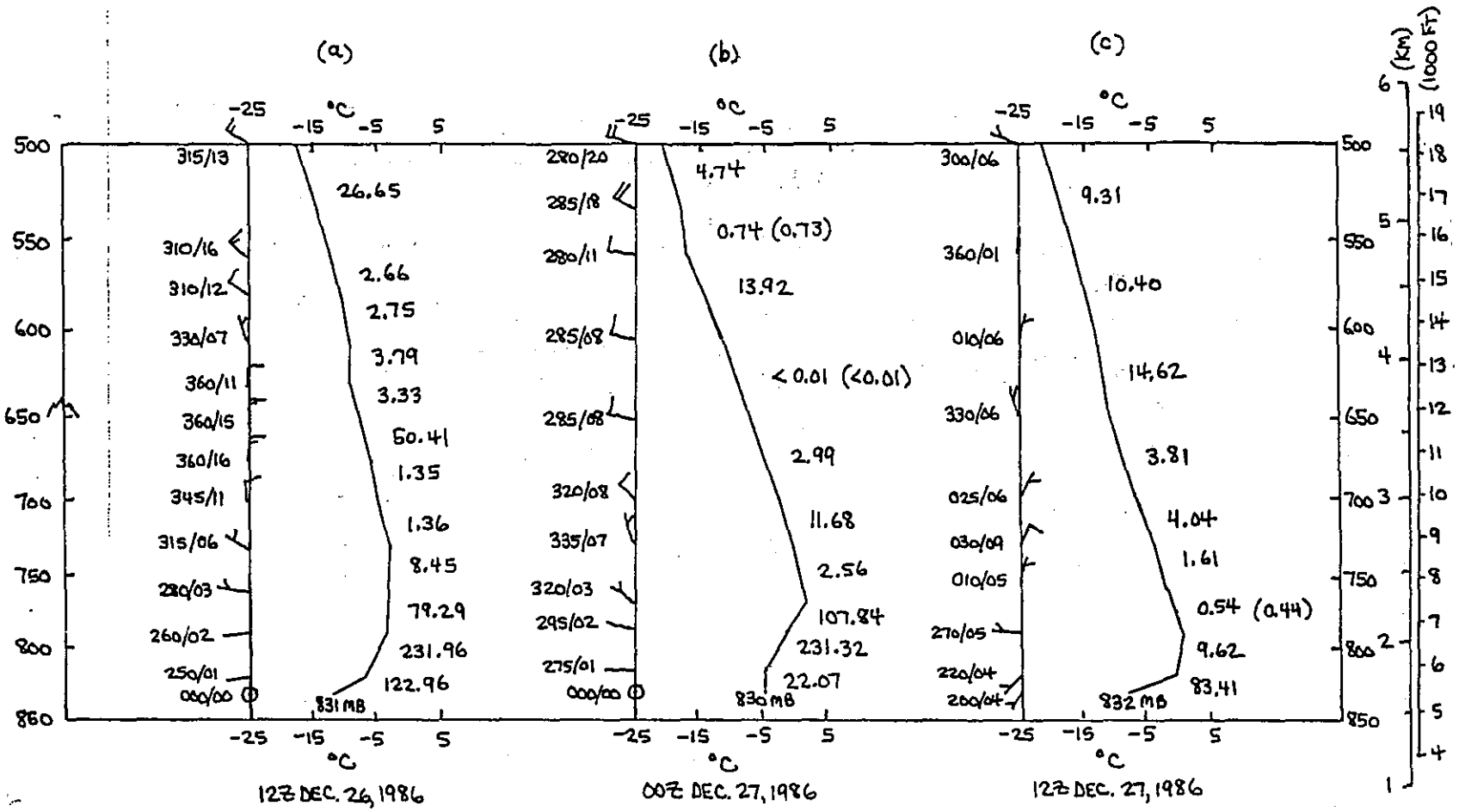

Fig. 22. Time-height variation of temperature (°C) and wind (DEG and kts) at Lander from surface to 500 mb for 12 UTC December 26, 00 UTC December 27, and 12 UTC December 27, 1986. Richardson numbers are to right of each temperature curve, and selected moist Richardson numbers are to the right of those in parentheses.

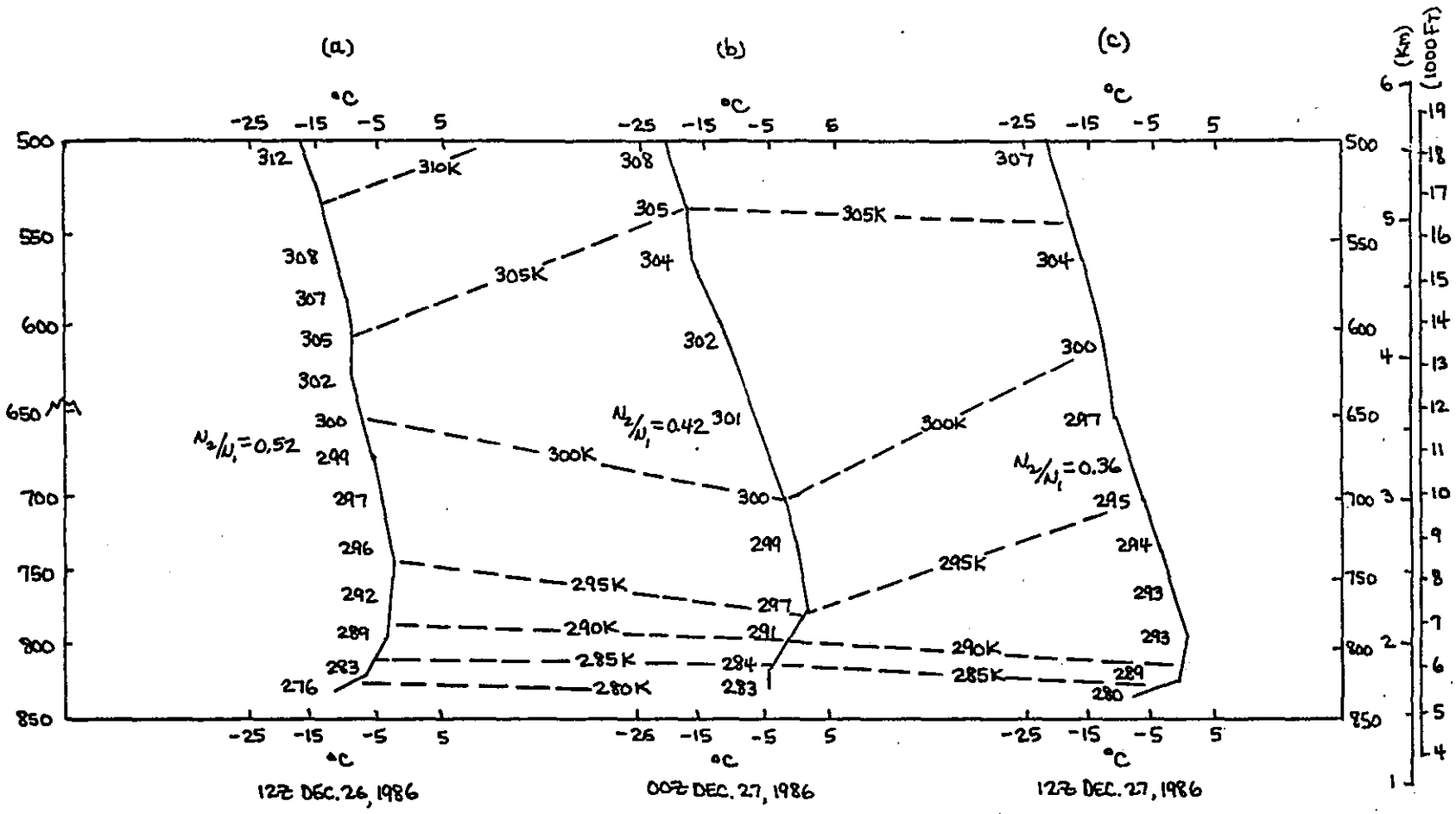

Fig. 23. Time-height variation of temperature (°C) at Lander from surface to 500 mb for 12 UTC December 26, 00 UTC December 27 and 12 UTC December 27, 1986. Potential temperatures (°K) are to left of each temperature curve.

As one would expect, wind directions below 700 mb during the day were veering, with little change in speeds or vertical wind shear. Richardson numbers remained stable (Fig. 22b). Figures 24a and b show wind shear values from the surface to 700 mb of 10.9 m sec^{-1} km^{-1} or less. This is in contrast to the values greater than 15 m sec^{-1} km^{-1} that were observed with the inversion-breaking cold frontal systems of the previous two cases. Although ACSL clouds were observed during the day (Fig. 25) indicating that mountain waves were occurring, they were likely at higher levels.

By 12 UTC December 27th the surface system was well to the east of the Wind River Basin. The trough extended from the Dakotas to the Nebraska Panhandle (Fig. 26). This is about coincident with the 500 mb thermal trough (Fig. 27). During the previous day the surface pressure at Lander had lowered from 831 mb to 830 mb. It then increased two millibars by 12 UTC December 27th. This is more than the normal diurnal change. From 03 UTC to 06 UTC a shift from west to southeast occurred in the surface winds (Fig. 25), however other changes were quite weak and inconclusive. Temperatures and dew points remained about the same after the wind shift, although there was about a millibar of pressure rise.

A distinct shift in the mid-level wind directions, a rising of the θ surfaces, and a change in the temperature profile indicate that a weak upper tropospheric cold front had passed through (Figs. 22, 23b and c). The front did not scour the stagnant air from the Basin. It was was not strong enough or deep enough. In fact, Figure 24c shows a temperature increase off the surface of 56°C km^{-1} --almost 50 percent greater than 24 hours earlier. Wind shear values remained relatively small (Fig. 24c) as did most of the Ri values remain high (Fig. 22c). This case lacked the critical elements for an inversion break--the passage of a strong, deep cold front capable of producing greater than 15 m sec^{-1} km^{-1} vertical shear and dynamic instability (i.e., Ri less than 0.25) in a layer near 700 mb.

5. Discussion

A. Moist Richardson Number

For these case studies, a moist Richardson Number, Rie, was calculated using the equivalent potential temperature, theta-e. Theta-e was chosen so that both the heats of condensation and evaporation would be included in the calculation. Even though the air masses associated with these stagnant episodes are normally dry, except in very shallow near surface layers, they can be associated with cloudiness, even precipitation.

On Figures 9, 14 and 22, if Rie values of 0.7 or less occurred, they were plotted to the right of Ri values in parentheses. As noted, Rie values were typically less than their corresponding Ri values. Figures 9 and 14 show instances where Ri > 0.25 and the corresponding Rie value was < 0.25. The fact that dynamic instability defined using the Rie criterion appears earlier than it would if the Ri one was used can be valuable in predicting an inversion break.

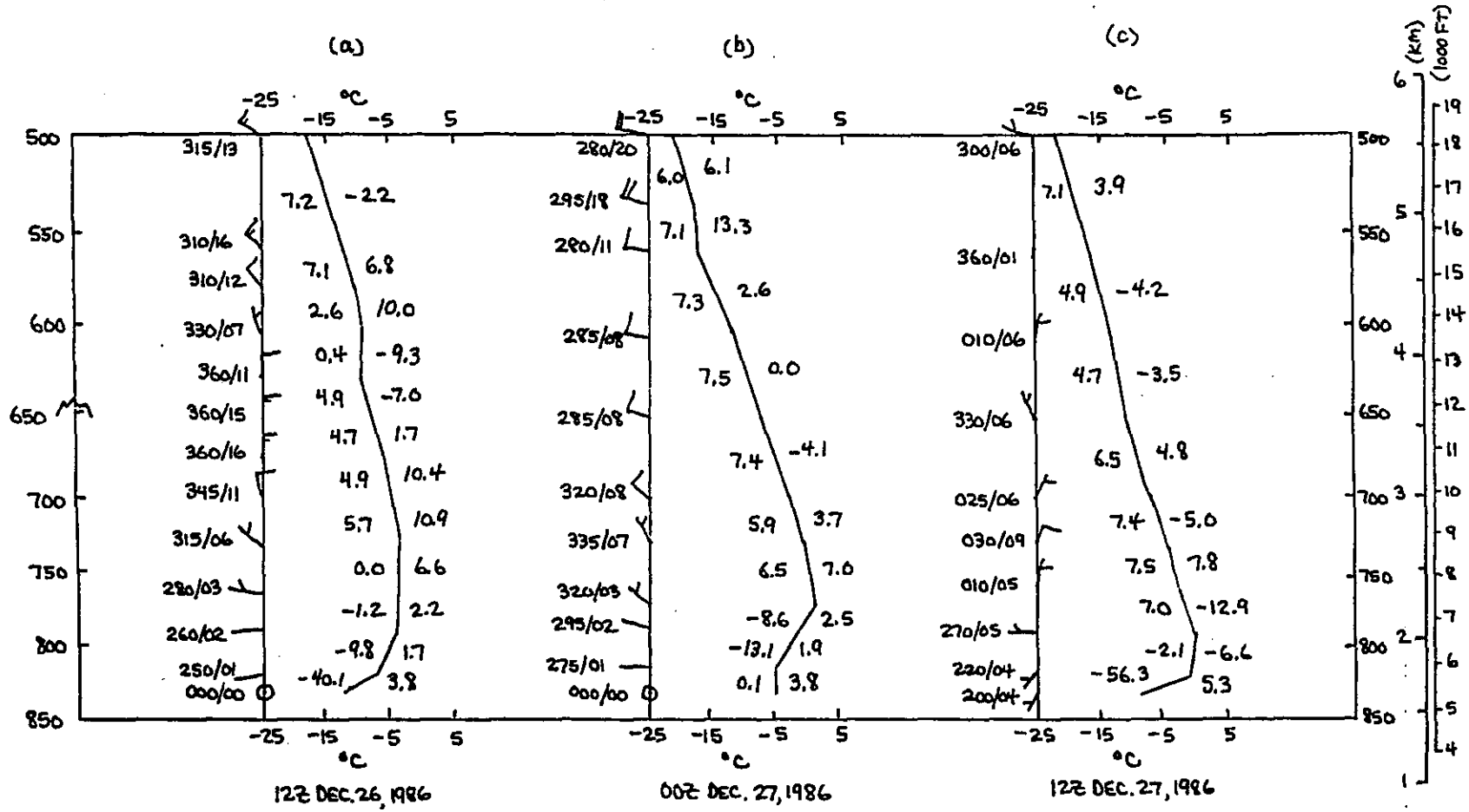

Fig. 24. Time-height variation of temperature (°C) and wind (DEG and kts) at Lander from surface to 500 mb for 12 UTC December 26, 00 UTC December 27, and 12 UTC December 27, 1986. Lapse rates (°C km^{-1}) are to the left of each temperature curve, and wind shear values (m sec^{-1} km^{-1}) to the right.

13 / 5 — 265 — 00 — 2/10 Cs

26/12Z

9 / 3 — 286 — 05 — 10/10 Cs

15Z

17 / 7 — 283 — 07 — 1/10 Ac 9/10 Cs

18Z

24 / 11 — 250 — -19 — FEW Ac 10/10 Cs

21Z

23 / 10 — 245 — -05 — FEW Acsl 9/10 Ac 1/10 Cs

27/00Z

19 / 9 / 13 — 260 — 03 — 7/10 Ac 3/10 Cs

03Z

18 / 13 — 244 — -03 — 4 — FEW Ac 10/10 Cs

06Z

20 / 12 — 245 — 08 — 6 — 10/10 Cs

09Z

17 / 11 — 254 — 03 — 2 — 4/10 Ac 6/10 Cs

27/12Z

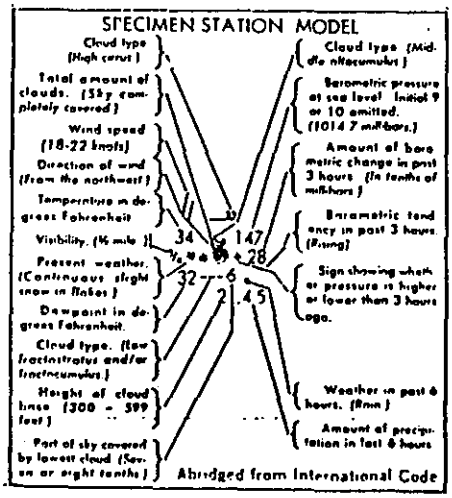

Fig. 25. Surface weather plot for Lander at three hour intervals from 12 UTC December 26 to 12 UTC December 27, 1986. Cloud amounts and types are to lower right of plot.

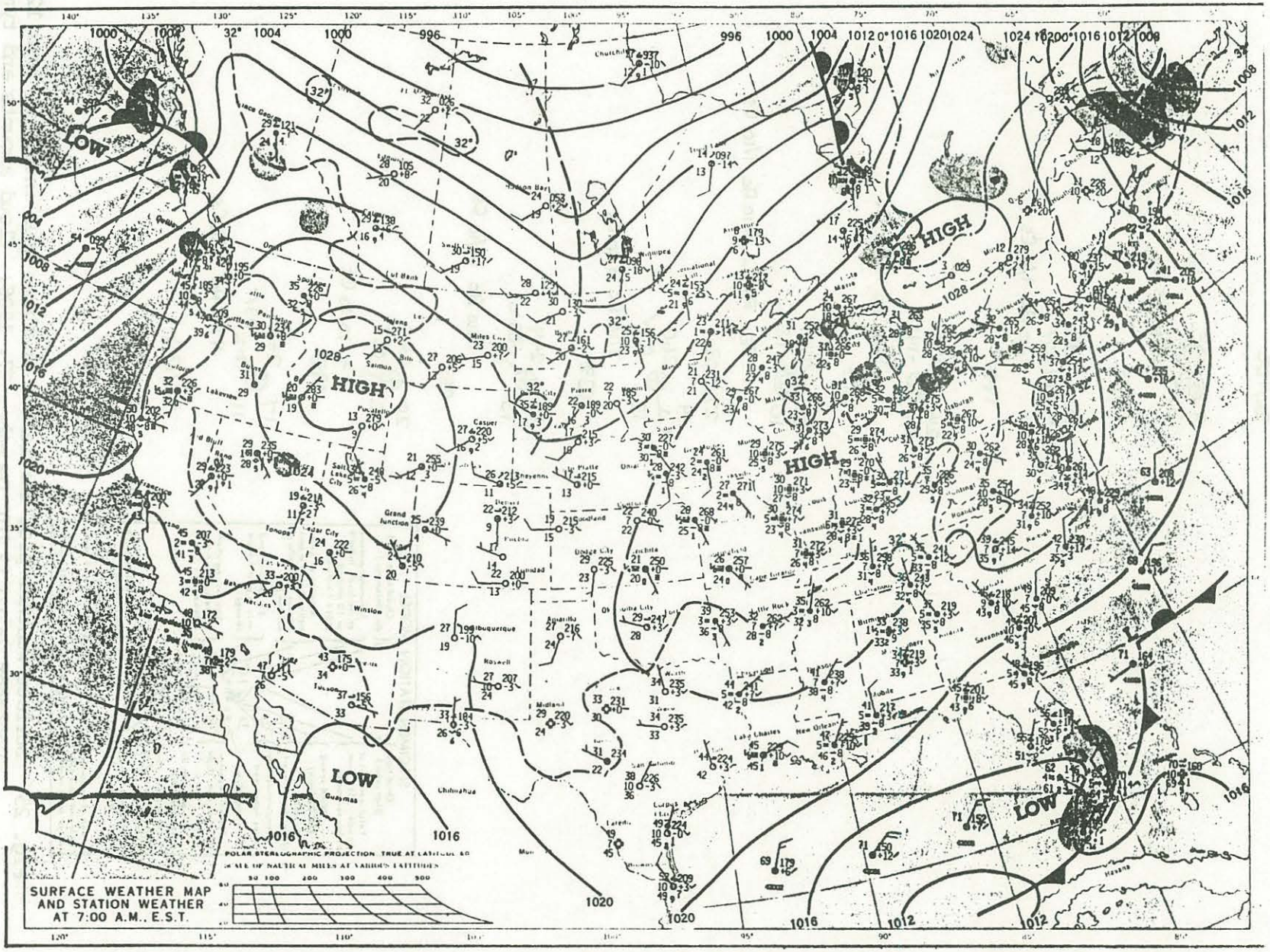

Fig. 26. Surface/sea level pressure analysis for 12 UTC December 27, 1986.

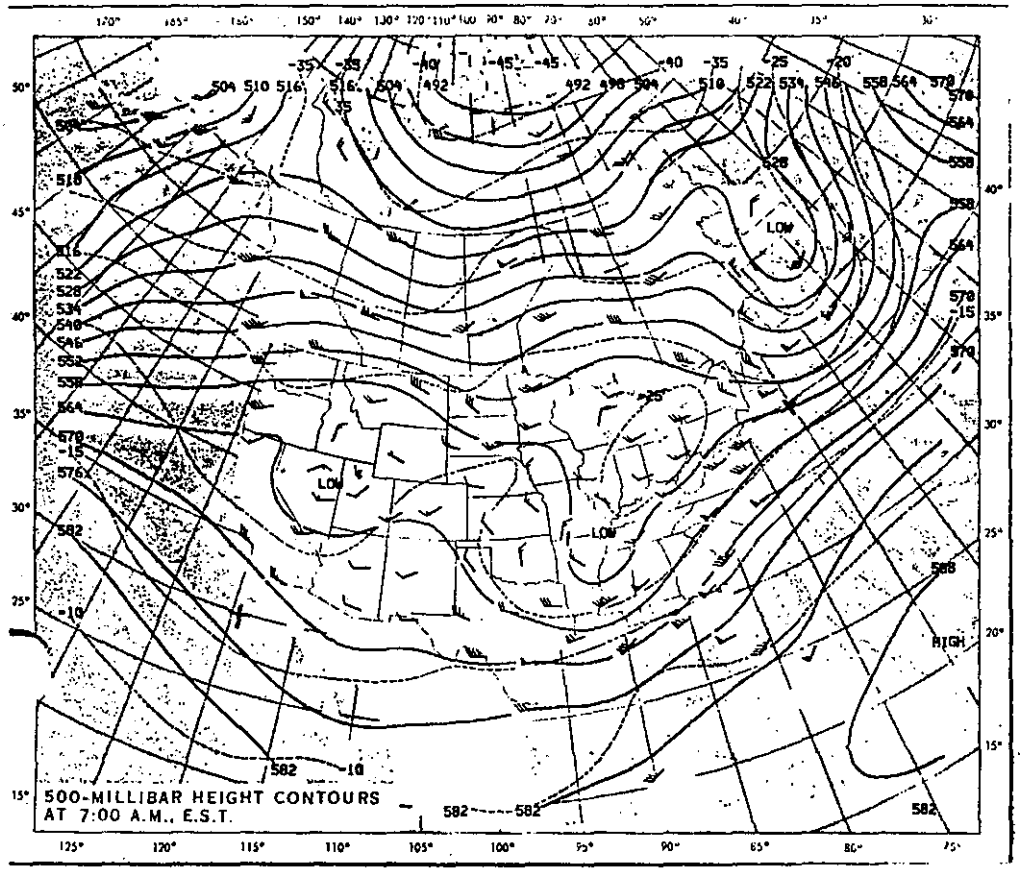

Fig. 27. 500 mb Chart for 12 UTC December 27, 1986.

However, the calculation of theta-e is complicated and requires the moisture profile. Thus, an attempt was made to statistically predict Rie values using Ri. Evaluation of over 60 (Ri, Rie) observation pairs with Ri less than or equal to one showed a correlation coefficient of 0.98 between the two parameters. A second order curve (Figure 28) yields a standard error of the Rie estimate of 0.25. Since the main aim is qualitatively assessing dynamic instability rather than quantitatively calculating Rie, this error is tolerable, although barely so.

The negative Ri values plotted on Figure 28 can be attributed to round off errors in the calculations or to weakly superadiabatic layers. No negative Ri values were found in the three cases discussed. A few cases of negative Richardson numbers were observed by Dalrymple et al. (1963), during the polar night, which they attributed to long wave radiation exchange with warm air aloft.

From the plot it is reasonable to assume that Rie is less than 0.25 when Ri is less than 0.68. This is in agreement with the cases presented. Thus, an Ri of 0.68 can be taken as the threshold of moist dynamic instability in the Wind River Basin.

B. Influence of Gravity Waves

Because of the number of dynamically unstable layers on the sounding immediately before and sometimes after inversion break, it appears that turbulent energy transfer develops prior to inversion break. This turbulence is an active mechanism which helps reduce the temperature discontinuity and static stability. Turbulent energy transfer adjusts the environmental lapse rate toward the dry adiabatic rate (Sutton, 1951). Gravity waves which form in the disturbed, dynamically unstable air flow off the Wind River Range are responsible for much of this turbulence. Typical streamlines and resulting turbulence downstream of mountains in cases of lee waves are shown in Figure 29.

Schaefer (1986) noted that gravity waves can be maintained only in an environment that features a layer with a Richardson number less that 0.5 which is at or near an altitude where wind speed equals the wave phase velocity, i.e., a critical level. The gravity wave induced horizontal velocity in a medium with shear is approximated by

$$u = U\ (\rho_o/\rho_t)^{-1/2} \quad \text{(Gossard \& Hooke, 1975)}$$

where U is the ambient wind speed, ρ_o is the density at the base of the strongly sheared layer and ρ_t is the density at the top of layer. Dynamic instability begins when Ri is less than 0.25, and in the cases studied this corresponds to

$$\theta_t - \theta_o \leq 1^\circ K$$

Considering the accuracy of calculation, this implies that

$$\theta_t \tilde{-} \theta_o \quad \text{over the unstable layer.}$$

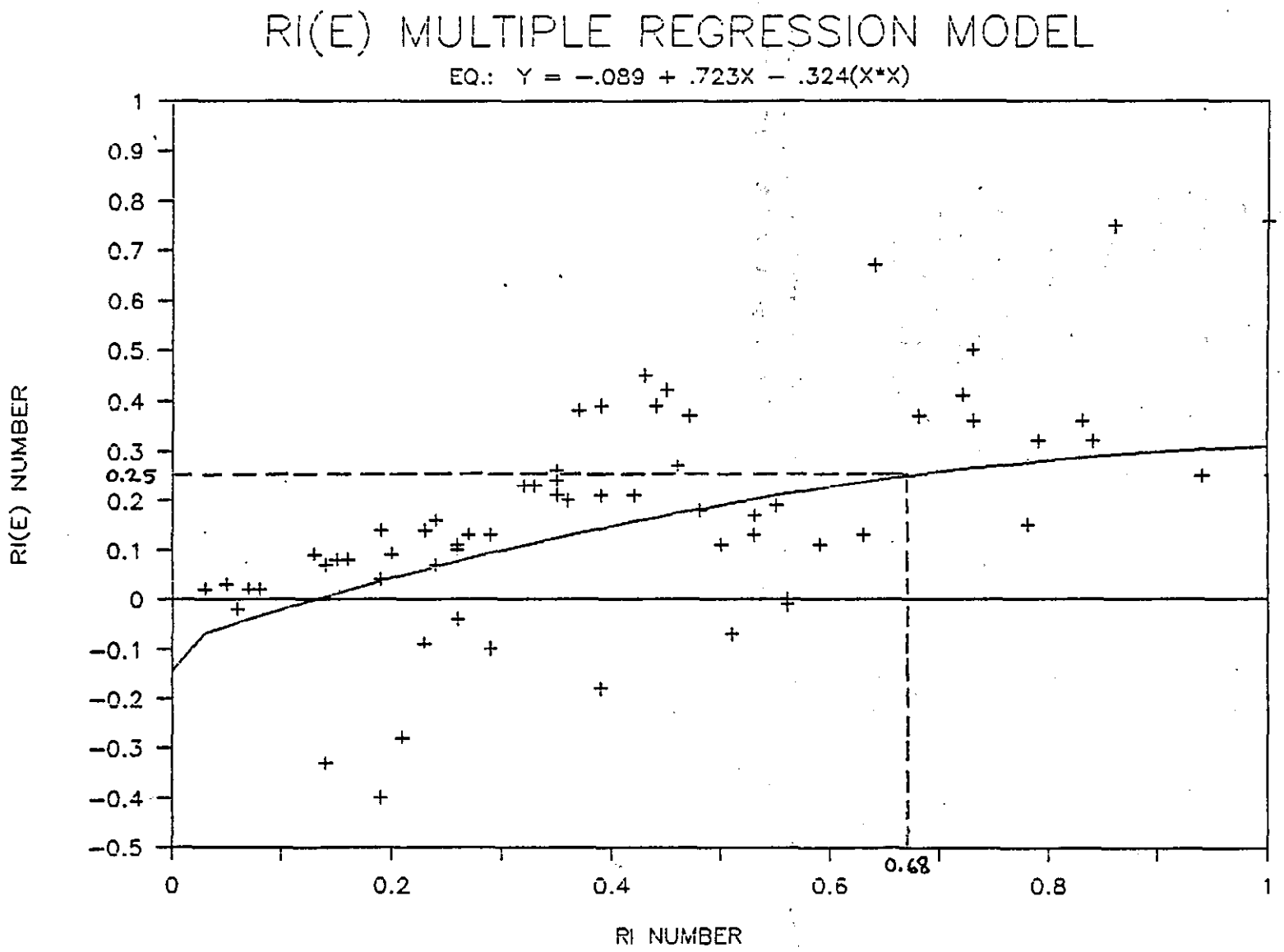

Fig. 28. Multiple regression model of Richardson Number (x-coordinate Ri) to Moist Richardson Number (y-coordinate Rie).

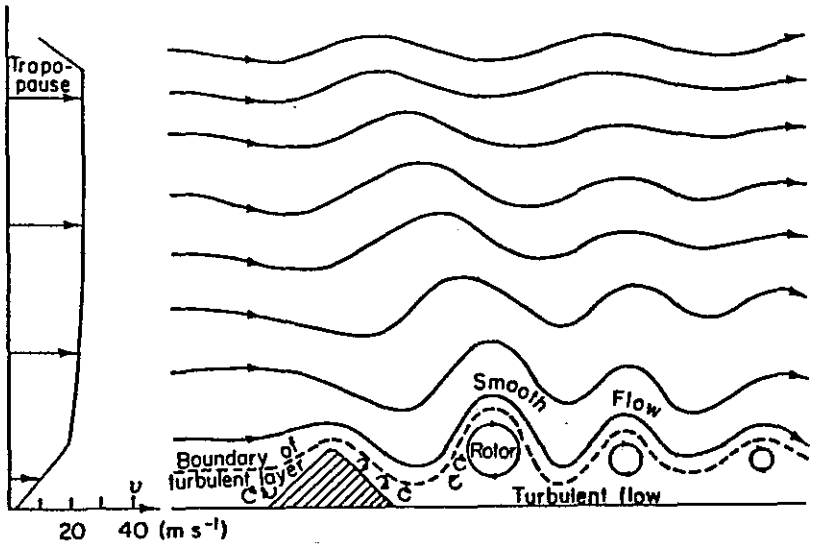

Fig. 29. Schematic diagram showing streamlines based on observed lee waves. The upstream velocity profile is indicated on the left (from Holton, 1979).

Since ρ_o/ρ_t is proportional to θ_t/θ_o, u approaches U, and a critical level exists. Thus, gravity waves can be maintained in the dynamically unstable layers.

Normally internal gravity waves moving in a quasi-horizontal layer of high stratification near the ground that is overlain by a deeper weakly stratified layer propagate their energy upward away from the surface. Fig. 30 schematically shows the normal relationship between the direction the gravity wave itself propagates and the direction the wave's energy propagates. This loss of energy causes low level disturbances associated with gravity waves to rapidly lose their amplitude. However, it is possible for wave refraction, and/or partial wave trapping to occur. Inversions are primary sites of wave trapping and ducting (Hooke, 1986) as shown in Figure 31. If wind shears are large (i.e., small Richardson number) wave over-reflections occur, that is the wave reflected from the critical layer has a larger amplitude than the incident wave itself (Hooke, 1986).

Both the vertical and horizontal atmospheric temperature structure affects wave propagation. This structure determines the frequency of internal gravity waves. This frequency is the Brunt-Vaisalla frequency and is given by:

$$N = (g\ d/dz(\ln\bar{\theta}))^{0.5}.$$

where the overbar represents an average over the wave containing layer. Thus, Brunt-Vaisalla is the square root of the numerator of an average Richardson number. For gravity wave energy to remain at low layers, the Brunt-Vaisalla frequency must decrease with height. Crook (1988) investigated the vertical temperature and wind profiles of several large amplitude gravity wave episodes detailed in the literature. The ratio of the Brunt-Vaisala frequencies for the weakly stratified upper layer and the lower highly stratified one (N2/N1) was approximately 0.3 for all the gravity wave events he studied.

This ratio was calculated for the cases in this study. N1 was calculated across the layer stretching from the surface to the top of the strong inversion, and N2 was calculated over a layer ranging upward from this point to 500 mb. The values are plotted on Figs. 10, 15 and 23. They range from 0.26 to 0.64. All of these are quite close to the 0.3 value. Further, if the 12 UTC December 30, 1986 value is recalculated with the bottom layer restricted to only the inversion layer, rather that the inversion layer plus the boundary layer, the high 0.64 ratio drops to a more compatible value of 0.36. These results indicate that low level gravity waves are a possible mechanism for turbulence production during scouring events.

However, note that there must exist some additional mechanism, besides the general stratification profile, to trap energy at low levels. Crook (1988) noted that there are three commonly occurring mechanisms: winds in the upper layer from a direction that opposes the wave motion; the existence of a jet in the lower layer that opposes the wave motion; and the existence of an elevated strong inversion at a height that maximizes the effects of wave reflection. Ideally, the inversion should be a quarter of a vertical wave length above the

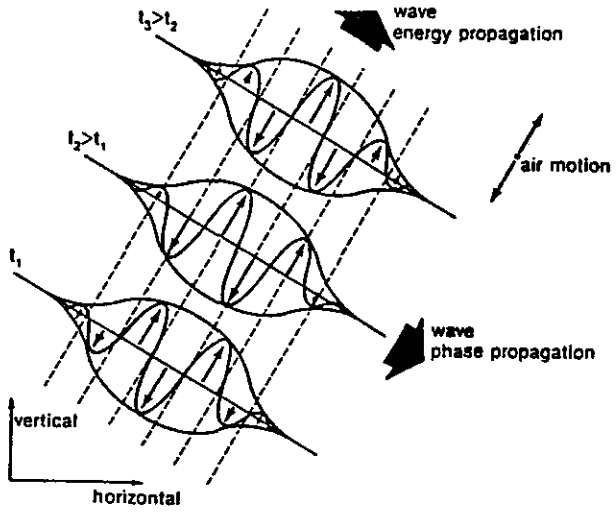

Fig. 30. Gravity wave energy and phase propagation (from Hooke, 1986).

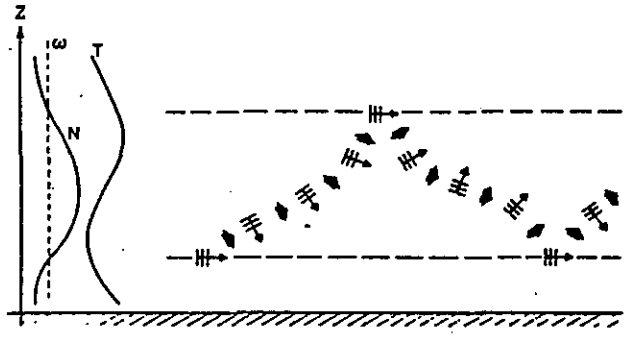

Fig. 31. Gravity wave trapping by inverted atmospheric temperature structure. The small arrows indicate phase propagation direction; the cross marks indicate the associated phase fronts and location of the gravity wave packet. Broad arrows indicate direction of packet motion (from Hooke, 1986).

ground. Further, the inversion should have a depth comparable to this height. Determination of this height is further complicated by the fact that the vertical wave length is a function of the horizontal one.

While this third mechanism is the most likely for the scouring of cold air from the Wind River Basin, the coarse horizontal resolution of the upper air network and the 12 hour interval between soundings make it virtually impossible to evaluate the wave lengths from operational synoptic data.

Whether trapped, or over-reflected, gravity waves act to extract available kinetic energy in the shear zone in which they are trapped or reflected. This decreases the potential temperature gradient through the layer, which is a reduction in static stability. Even when gravity waves are evanescent, and not ducted, so that their amplitude decreases exponentially with distance away from the critical level, significant amounts of energy can be propagated (Schaefer, 1988). In the case of low level opposing flow, Crook (1988) found vertical velocities of 1 to 1.5 m sec^{-1} generated by the gravity waves.

In addition to stagnant unconditionally stable winter air masses, the action of gravity waves has application to severe thunderstorm environments (Uccellini, 1975). If gravity waves can act to remove temperature discontinuities, they could erode a capping inversion and permit stalled convection to again become positively buoyant.

6. Summary

Inversion breaks almost entirely occur in the interval between the 00 UTC and 12 UTC soundings. One would assume this is a direct result of the time-of-day that wintertime cold fronts most frequently pass through the Wind River Basin. When an approaching tropospheric disturbance, usually a Pacific or Canadian cold front with cold air advection from surface to upper troposphere, produces the following conditions there is a strong likelihood that any stagnant air mass in the Basin will be replaced:

1. Greater than 15 m sec^{-1} km^{-1} vertical wind shear in a layer from the surface to about 700 mb. This wind shear requirement amounts to about 10 kts of speed increase through a 1,000 feet unstable layer. Wind directions are generally from the west quadrant, i.e., southwest, west, or northwest.

2. There is a low level layer that is dynamically unstable with Ri or Rie less than 0.25. (Ri less than 0.7 can be taken as the onset of instability.) The dynamic instability usually first occurs in a layer immediately above or below the 700 mb level, i.e., near the level of the top of the upstream mountain range.

Typically only a mature surface to upper tropospheric frontal system is sufficiently strong to satisfy the vertical wind shear and Richardson Number requirements. The passage of a very strong cold front produces a most dramatic surface temperature increase--about 10°F hr^{-1} for one or two hours. Warmings of as much as 46°F in one hour have been recorded at Lander. Fronts of marginal

strength, but still able to break the inversion, will produce only about 5° to 10°F warming over several hours. Only after the initial burst of warming do the characteristics of the new air mass begin to show.

Following cold frontal passage, the greater the snow depth (four inches or more), and the colder and drier the new air mass, the more likely the new air mass is to become trapped in the Wind River Basin. The longer days and shorter nights of spring bring a final end to the cycle.

7. Acknowledgements

The authors wish to thank Dr. Joseph T. Schaefer, Central Region Scientific Services Division, for his patience and guidance in the writing of this paper. Also, Scott A. Mentzer, WSFO Cheyenne, aided in developing a computer program to analyze the data.

8. References

Anon, 1969: Use of the Skew T, Log P Diagram in Analysis and Forecasting. Air Weather Service Manual 105-124, Headquarters, AWS(MAC), Scott AFB, Illinois, 130 pp.

Browning, K. A., Harrold, T. W., and J. R. Starr, 1970: Richardson number limited shear zones in the free atmosphere. Quart. J. Roy. Meteor. Soc., 96, 40-49.

Browning, K. A., and T. W. Harrold, 1970: Air motion and precipitation growth at a cold front. Quart. J. Roy. Meteor. Soc., 96, 369-389.

Crook, N. A., 1988: Trapping of low-level internal gravity waves. J. Atmos. Sci., 45, 1533-1541.

Dalrymple, P. C., Lettau, H. H., and Wollaston, S. H., 1963: South Pole micrometeorology program, Rep. No. 20, 94 pp. Inst. Polar Studies, Ohio State Univ., Columbus, Ohio (ES-7).

Einaudi, F., and D. P. Lalas, 1974: Some new properties of Kelvin-Helmholtz waves in an atmosphere with and without condensation effects. J. Atmos. Sci., 31 1995-2007.

Gossard, E. E., and W. H. Hooke, 1975: Waves in the Atmosphere. Elsevier Scientific, Amsterdam, 456 pp.

Haltiner, G. J., and F. L. Martin, 1957: Dynamical and Physical Meteorology. McGraw-Hill, New York, 470 pp.

Hess, S. L., 1959: Introduction to Theoretical Meteorology. Holt, Rinehart and Winston, New York, 362 pp.

Holton, J. R., 1979: An Introduction to Dynamic Meteorology. Academic Press, New York, 319 pp.

Hooke, W. H., 1986: Gravity Waves. Mesoscale Meteorology and Forecasting. P. S. Ray (ed.). American Meteorological Society, Boston, 272-288.

Huschke, R. E. (ed.), 1959: Glossary of Meteorology. American Meteorological Society, Boston, 482-483.

Lalas, D. P., and F. Einaudi, 1973: On the stability of a moist atmosphere in the presence of a background wind. J. Atmos. Sci., 30, 795-800.

Lilly, D. K., 1986: Instabilities. Mesoscale Meteorology and Forecasting. P. S. Ray (ed.). American Meteorological Society, Boston, 259-271.

Ludlam, F. H., 1967: Characteristics of billow clouds and their relation to clear-air turbulence. Quart. J. Roy. Meteor. Soc., 93, 419-435.

Munn, R. E., 1966: Descriptive Micrometeorology. Academic Press, New York, 245 pp.

Reiter, E. R., and P.F. Lester, 1967: The Dependence of the Richardson Number on Scale Length. Atmospheric Science Paper No 111, Colorado State U., Ft. Collins Co., 39 pp

Schaefer, J. T., 1986: The Dryline. Mesoscale Meteorology and Forecasting. P. S. Ray (ed.). American Meteorological Society, Boston, 549-572.

Sellers, W. D., 1965: Physical Climatology. University of Chicago Press, Chicago, 272 pp.

Shapiro, M. A., 1974: A multiple structured zone-jet stream system as revealed by meteorologically instrumented aircraft. Mon. Wea. Rev., 102, 244-253.

Sutton, O. G., 1951: Atmospheric Turbulence and Diffusion. Compendium of Meteorology. T. F. Malone (ed.). American Meteorology Society, Boston, 492-509.

Uccellini, L. W., 1975: A case study of apparent gravity wave initiation of severe convective storms. Mon. Wea. Rev., 103, 497-513.